

Quantum dot spin qubits in Silicon: Multivalley physics

Dimitrie Culcer,¹ Łukasz Cywiński,^{1,2} Qiuzi Li,¹ Xuedong Hu,^{1,3,4} and S. Das Sarma¹

¹*Condensed Matter Theory Center, Department of Physics,
University of Maryland, College Park MD 20742-4111*

²*Institute of Physics, Polish Academy of Sciences,
al. Lotników 32/46, PL 02-668 Warszawa, Poland*

³*Joint Quantum Institute, Department of Physics,
University of Maryland, College Park MD 20742-4111*

⁴*Department of Physics, University at Buffalo, SUNY, Buffalo, NY 14260-1500*

The long spin coherence times measured in Si have brought single-spin and singlet-triplet qubits in Si quantum dots at the focus of an energetic experimental effort. One potential obstacle to Si quantum computation is the role of the valley degree of freedom. Although confinement and uniaxial strain at the interface partially lift the valley degeneracy, so that only the two valleys perpendicular to it need to be considered, the size of the orbital spectrum is greatly increased. Scattering at the interface also produces a valley-orbit coupling of magnitude Δ between these two lowest-lying valleys, yet Δ is generally unknown *a priori* because it depends on detailed knowledge of the interface. In this work we study single-spin and singlet-triplet qubits in silicon double quantum dots, accounting fully for the valley degree of freedom and assuming no prior knowledge of the valley-orbit coupling Δ . For a valley splitting $\Delta \ll k_B T$, when the valleys are effectively degenerate, neither scheme can be operational, while for a valley splitting $\Delta \gg k_B T$ qubits can be implemented in both schemes. For single-spin qubits we analyze the spectrum of a multivalley double quantum dot, identify the conditions for the lowest energy two-electron states to be a singlet and a triplet well separated from other states, and determine the magnitude of the exchange splitting. For singlet-triplet qubits we analyze the single-dot spectrum and initialization process, as well as the double-dot spectrum, mixing in an inhomogeneous magnetic field and spin blockade. We show that quantum-coherent experiments may provide an alternative method for estimating the valley coupling in Si. We consider the possibility of valley mixing under the action of the hyperfine interaction, and address briefly the situation in which the valley-orbit coupling is different in each dot due to interface roughness.

I. INTRODUCTION

Quantum computation stands out as a vibrant and expanding area of research in contemporary physics. Investigations of computation based on the rules of quantum mechanics, comprising unitary evolution, entanglement and superposition, are continually exploring novel facets of physics and information science, while providing new perspectives on older problems as well. For example, quantum computers (QC) are believed to have the potential to enhance computational power for certain problems and to offer increased functionality¹.

A practical QC architecture requires scalability and long coherence times. Spin-based solid state quantum bits (qubits) are known to have long coherence times,^{2,3} while also offer promise of scalability, are natural candidates for quantum computation. Phosphorus donors in Silicon are known since 1950s to have one of the best spin coherence properties in solids,⁴ and were therefore proposed as a viable candidate for qubit.⁵ However, fabrication of ordered and gated donor arrays and coherent control over donor electrons turned out to be extremely difficult (note nevertheless outstanding recent developments^{6,7}). On the other hand, spin qubits in quantum dots (QDs)⁸, particularly in GaAs, have been actively studied in the past decade. Various schemes exist for implementing spin qubits in QDs. For the original single-spin qubits, one electron spin is initialized in each dot in a QD array, with spin up and down represent-

ing the two states of a qubit.⁸ One-qubit rotations are accomplished using magnetic resonance techniques and two-qubit rotations by means of a pulsed exchange interaction. One can also use selected two-spin states to encode a logical qubit. For example, in singlet-triplet qubits it is the singlet and unpolarized triplet states that are used for encoding. Here exchange coupling gives the splitting of the two-spin states making up the qubit. One-qubit rotations are currently carried out using an inhomogeneous magnetic field across the two dots and pulsed exchange splitting. The inhomogeneous field is obtained in GaAs from nuclear spin polarization, though in the future a nanomagnet may also be used for increased control.² Notice that exchange coupling plays a different role in the two schemes. Two-qubit operations have been described in Refs. 9,10 while developments in achieving control over the inhomogeneous Overhauser field were reported in Ref. 11. Last but not least, larger encoding schemes such as using three-spin states have also been proposed,¹² which promises an all-electrically-controlled architecture.

Recent years have seen significant experimental progress involving single-spin properties such as coherent control, coherence, and measurement.^{3,13–21} In particular in GaAs double quantum dots (DQDs) spin blockade¹³ and charge sensors (quantum point contacts and radio-frequency quantum point contacts)²² enable observation of single/two-spin dynamics.^{2,3,16,17,23} Spin coherence in GaAs QDs is mostly limited by hyperfine interaction with

the nuclear spins,^{24–32} although there have been various proposals for manipulating the nuclear spin states in order to extend electron spin coherence times,^{33–36} and recent experiments² have shown that dynamical decoupling schemes^{27,32,37–40} could help unwind the nuclear spin dynamics and extend the electron spin coherence time. Silicon on the other hand has outstanding spin coherence properties⁴ due to small spin-orbit coupling,⁴¹ small hyperfine interaction with nuclear spins⁴² (which can be reduced by isotopic purification⁴³) and absence of piezoelectric coupling.⁴⁴ The spin coherence time T_2 (after Hahn spin echo) for donor electron spins in bulk Si:P has been reported to range from 60 ms⁴⁵ to 300 ms.⁸⁵ This is the longest coherence time measured in electron spin qubits, and greatly exceeds⁸⁶ the $\sim 1\mu\text{s}$ reported in GaAs QDs.^{2,3} The technique of isotopic purification of Si, where ^{29}Si nuclei are preferentially removed in favor of ^{28}Si and ^{30}Si nuclei from natural Si, allows for the practical possibility of indefinite enhancement of Si electron spin coherence time, something that simply cannot be done in GaAs.^{45,46} This possibility of isotopic purification makes Si electron spin an ideal solid state qubit which, as a matter of principle, can be completely free of quantum decoherence. In addition to the maturity and continuous innovation in Si microfabrication technology could be of great help in scaling up a Si-based QC architecture. At present work is under way on several proposed Si QC architectures. These include architectures based on donor electron or nuclear spins in a Si:P system,^{5,47} single electron spins in gate-defined quantum dots in Si/SiGe^{48,49} or Si/SiO₂,^{50–52} and SiGe nanowires.¹⁸ Experimental progress has been made in both donor-based devices^{6,7,53–59}, and gate-defined quantum dots^{19,50,51,60–63} with significant developments within the past year.

One of the biggest obstacles to spin QC in Si is the valley degree of freedom. In bulk Si there are six degenerate conduction band minima, which complicate the orbital and spin state spectrum. For example, in Si QC schemes based on Si:P donors it is necessary to take into account valley interference effects in spin interactions.⁶⁴ In this case impurity scattering breaks the symmetry of the lattice and allows coupling between the valleys. In samples in which two or more donor centers are present interference becomes possible and is sensitively dependent on the exact atomic locations of the two donors. This problem has also been studied beyond the effective mass approximation,⁶⁵ showing that part of the interference is smoothed out when one uses a set of basis functions spanning many wave vectors around the valley edges.

The presence of an interface partially lifts the sixfold valley degeneracy. Uniaxial tensile strain at the interface and/or confinement in the \hat{z} -direction cause the valleys perpendicular to the interface to have a smaller energy by several tens of meV than the valleys in the plane of the interface. In other words, at the interface only two valleys are relevant to the ground orbital state. The interface

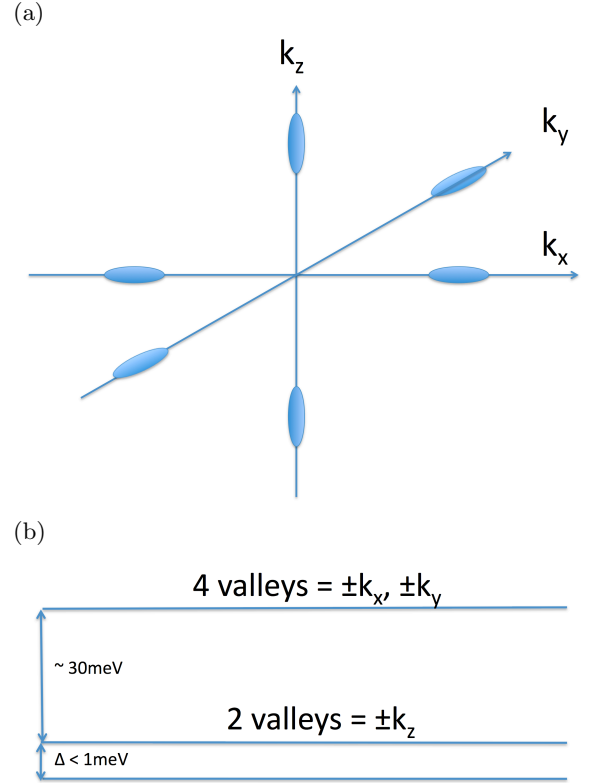


Figure 1: (color online) Conduction-band valleys in silicon in the bulk and in 2D. (a) In bulk Si there are six equivalent conduction-band minima positioned along the Cartesian axes. (b) Uniaxial strain at the interface causes the valleys parallel to the interface (i.e. in the xy -plane here) to be higher by several tens of meV than the valleys perpendicular to the interface. The interface potential further splits the lower-energy valleys by an amount Δ , which present experimental work is striving to determine unambiguously. Based on measurements to date we expect $\Delta < 1\text{meV}$.

further couples the two z -valleys by producing a valley-orbit coupling Δ . Valley-orbit coupling causes quantum dot orbitals to hybridize, as pointed out by Ando for electrons in a quantum well.⁶⁶ The magnitude of Δ is generally not known *a priori*, and is sample-dependent.⁶⁷ It is also different for different interfaces, such as Si/SiGe and Si/SiO₂. At present there is no standard experiment to measure the valley splitting for a quantum dot. Measurement of Δ is generally done for a two-dimensional electron gas (2DEG) at high magnetic fields, and the zero-field valley splitting is then obtained via extrapolation,⁸⁷ see e.g. Ref. 68. Valley splitting measurements have also been reported at low fields⁶¹ and experimental efforts in this direction are continuing. A large valley splitting was recently reported in Si/SiO₂⁶⁹ and is attributed to the high-quality interface, though further work is needed to confirm this claim. Motivated by QC considerations, multiple efforts have also been devoted to calculating the valley splitting.^{48,67,70–73}

In this work we analyze spin qubits in multivalley Si

QDs within the effective mass approximation. The discussion of valley physics is general and applies to all types of Si QDs, yet when concrete figures are needed we focus on Si/SiO₂. Let us also mention that many aspects of the following considerations apply also to carbon-based QDs, where the valley degree of freedom is present as well.^{74,75} We consider first single-spin qubits, i.e. the Loss-DiVincenzo (LDV) architecture,⁸ as in Fig. 2 (a). We determine the spectrum and the conditions required for implementing single-spin qubits and coupling adjacent qubits by means of the exchange interaction. For a valley splitting $\Delta \gg k_B T$ one effectively has a single-valley problem, in which two-qubit manipulations using two-spin singlet and triplet states can be carried out exactly as in GaAs. On the other hand if the valleys are degenerate then the lowest two-electron states are a degenerate singlet and triplet.⁷⁶ The ability to carry out quantum information processing thus depends sensitively on the single-spin states that are initialized in the two dots. If the spins on the two dots are initialized in the same valley one has nonzero exchange between the singlet and the triplet. Yet, since one cannot prepare single electron states with absolute certainty about the orbital part, it is not possible to determine *a priori* what the exchange will be when electrons are allowed to tunnel between dots. This implies that the size of Δ is important during initialization, as long as the interactions turned on during two-spin manipulation do not couple the valleys. Once a certain valley eigenstate is initialized, qubit manipulation will be straightforward as long as further valley-orbit coupling or intervalley scattering are not introduced by the barrier potential or by the electron-electron Coulomb potential. In other words, even if a lower-energy valley eigenstate exists, the originally initialized two-spin valley state will not adiabatically evolve into it.

We subsequently study singlet-triplet qubits,^{2,9} as in Fig. 2 (b). As part of our discussion we analyze the feasibility of an experiment analogous to Ref. 2 in a Si/SiO₂ (or Si/SiGe¹⁹) DQD. The valley degree of freedom affects qubit initialization, operation,⁷⁷ and spin blockade.⁷⁵ For $\Delta \gg k_B T$ a singlet-triplet qubit can be implemented in the same way as in GaAs. For $\Delta \approx k_B T$ significant problems may be encountered in attempting to initialize the qubit, since, unlike in GaAs, the energy scale is no longer set by the confinement energy but by the valley splitting.

Once a qubit is initialized it can be manipulated using an inhomogeneous magnetic field. In general this inhomogeneous field will be composed of the Overhauser field of the nuclei and an external applied magnetic field. The latter does not mix states with different valley composition, while the former can induce transitions between

valley eigenstates, yet these coupling occur on long time scales in Si and do not affect quantum computation. We demonstrate that the mixing of singlet and triplet states induced by the inhomogeneous magnetic field is analogous to the situation in GaAs. Despite the large number of states, only a few states can mix among themselves. Moreover, spin blockade also occurs in a manner analogous to GaAs. Sweeping a magnetic field brings out the multivalley structure of the ground state and the fundamental complications it introduces in distinguishing spin and orbital degrees of freedom. As the magnetic field is increased a clear transition occurs from the pseudospin structure at large valley splittings to the Zeeman structure at large magnetic fields. We further show that a series of experiments analogous to Ref. 2 should provide a direct way to estimate the valley splitting Δ by sweeping a magnetic field and measuring the average probability of return over many experimental runs.

The outline of this article is as follows. In Sec. II we introduce the Hamiltonian for the DQD and discuss the wave functions and the valley-orbit coupling. In Sec. III we study the effect of the valley degree of freedom on single-spin qubits using the Hund-Mulliken molecular orbital method. In Sec. IV we investigate singlet-triplet qubits and the role of the valley degree of freedom in initialization, coherent manipulations, and readout. Special attention is paid to mixing in an inhomogeneous magnetic field, and in Sec. V it is shown that a series of quantum coherent experiments can provide a way of estimating the valley splitting. We also discuss briefly the effect on spin qubits of interface roughness, which may lead to a different valley-orbit coupling in the two dots. We end with a summary and conclusions.

II. MODEL OF DOUBLE QUANTUM DOT

Our focus throughout this paper is on a DQD in a two-dimensional electron gas (2DEG) formed in the inversion layer of a MOSFET structure that is taken to be grown along the \hat{z} -direction (which is also the crystalline (001) direction). The dots are located at $\mathbf{R}_D = (X_D, 0, 0)$, where $D = L, R$, and $X_R = X_0$ while $X_L = -X_0$ (since the \hat{z} and $-\hat{z}$ valleys are isotropic in the xy plane, we can choose the \hat{x} and \hat{y} axes by convenience). The Hamiltonian describing the double-dot system is written as $H = H_0 + \sum_{i=1,2} H_v^{(i)}$, where H_v represents the valley-orbit coupling discussed below and $H_0 = (\sum_{i=1,2} T^{(i)} + V_Q^{(i)}) + V_{ee}$, where T is the kinetic energy operator and V_Q the confinement potential

$$V_Q = \frac{\hbar\omega_0}{2a^2} \text{Min}[(x - X_0)^2, (x + X_0)^2] - eEx + \frac{\hbar\omega_0}{2a^2} y^2 + \frac{\hbar\omega_z}{2b^2} z^2, \quad (1)$$

with a and b the Fock-Darwin radii for in- and out-of-plane confinement respectively. The external electric field $\mathbf{E} \parallel \hat{\mathbf{x}}$ can be used to bias one dot with respect to the other and is relevant in the case of singlet-triplet qubits discussed below. The Coulomb potential between electrons at \mathbf{r}_1 and \mathbf{r}_2 is $V_{ee} = e^2/(\epsilon|\mathbf{r}_1 - \mathbf{r}_2|)$, where the effective dielectric constant $\epsilon = (\epsilon_{\text{Si}} + \epsilon_{\text{SiO}_2})/2$, accounting for the effect of the image charge in the substrate SiO_2 layer (for Si/SiGe heterostructures such averaging would not be needed). The confinement potential for each dot is harmonic, with the single-dot potentials $V_D(x) = (\hbar\omega_0/2a^2)(x - X_D)^2$, and ground states are both Gaussian.

The six degenerate valleys of bulk Si, i.e. equivalent conduction band minima, are located along the $\langle 100 \rangle$ crystal directions towards X points. Confinement at the Si/SiO₂ interface splits them into a doubly-degenerate branch of lower energy and a fourfold-degenerate branch of higher energy. The two lower energy valleys are along the direction perpendicular to the interface at $\mathbf{k}_\xi = \pm k_0 \hat{\mathbf{z}}$, where $\xi = z, \bar{z}$ indexes the two valleys, $k_0 = 0.85(2\pi/a_{\text{Si}})$, and the lattice constant $a_{\text{Si}} = 5.43\text{\AA}$. The ground-state single-electron wave functions D_ξ represent either of the degenerate $\pm k_0$ valleys on the left and right dots respectively. On either dot $(T + V_D)D_\xi = \varepsilon_0 D_\xi$, with $D_\xi = F_D(\mathbf{r} - \mathbf{R}_D)e^{i\mathbf{k}_\xi \cdot \mathbf{r}}u_\xi(\mathbf{r})$, with $D = L$ or R . The envelope functions are

$$F_D(\mathbf{r} - \mathbf{R}_D) = \frac{1}{\pi^{3/4}(a^2b)^{1/2}} e^{-\frac{(x-X_D)^2}{2a^2}} e^{-\frac{y^2}{2a^2}} e^{-\frac{z^2}{2b^2}}, \quad (2)$$

where $a = \sqrt{\frac{\hbar}{m_t\omega_0}}$ is the in-plane Fock-Darwin radius and b is the growth-direction confinement length. Here $m_t = 0.191m_0$ is the in-plane (transverse) Si effective mass, with m_0 the bare electron mass. The lattice-periodic part of the Bloch function can be written as $u_\xi(\mathbf{r}) = \sum_{\mathbf{K}} c_{\mathbf{K}}^\xi e^{i\mathbf{K} \cdot \mathbf{r}}$ with \mathbf{K} representing the reciprocal lattice vectors.

The overlap between states on the two dots belonging to the same valley is $l = \langle L_\xi | R_\xi \rangle = e^{-d^2}$, where $d = X_0/a$ is the dimensionless half-interdot-distance. Overlaps between states from different valleys, of the form $\langle D_\xi | D_{-\xi} \rangle$, are negligible. They are suppressed by an exponential of the form $e^{-\frac{b^2 Q_z^2}{4}}$, where $Q_z = \frac{2\pi n_z}{a_{\text{Si}}} - 2k_0$ (n_z is an integer), which is easily verified to be $\ll 1$. For example, b is typically on the order of 3 nm,⁷⁸ giving $b^2 Q_z^2/4 \approx 800$ when $n_z = 0$ and ≈ 150 when $n_z = 1$. Matrix elements of smooth (in space) potentials and interactions between states from different valleys are generally suppressed by such exponential prefactors. Thus single-particle matrix elements of the form $\langle D_\xi | H_0 | D_{-\xi} \rangle$ are suppressed, as are two-particle matrix elements of the form $\langle D_\xi^{(1)} D_\xi^{(2)} | H_0 | D_{-\xi}^{(1)} D_{-\xi}^{(2)} \rangle$. The one exception is the matrix element referred to as the valley-exchange Coulomb integral, which is discussed in detail in Appendix D. Two-particle matrix elements in which each electron belongs to a different valley, for example

$\langle D_\xi^{(1)} D_{-\xi}^{(2)} | H_0 | D_\xi^{(1)} D_{-\xi}^{(2)} \rangle$, are of the same order of magnitude as those in which all functions belong to the same valley, such as $\langle D_\xi^{(1)} D_\xi^{(2)} | H_0 | D_\xi^{(1)} D_\xi^{(2)} \rangle$. All these matrix elements are given in Appendix A.

Notice that matrix elements of any interaction that has atomic length scale is not exponentially suppressed. One prominent example is the contact hyperfine interaction between a conduction electron and a ²⁹Si nuclear spin (in a natural Silicon substrate about 5% of the nuclei are ²⁹Si): $H_{\text{HF}} = \sum_i \mathcal{A} \nu_0 \mathbf{S} \cdot \mathbf{I}_i \delta(\mathbf{r} - \mathbf{R}_i)$, where the sum runs over the positions of the ²⁹Si nuclei, \mathcal{A} is the hyperfine coupling, ν_0 is the unit cell volume, and \mathbf{I}_i are the nuclear spins. For this Hamiltonian $\langle D_\xi | H_{\text{HF}} | D_{-\xi} \rangle = \mathcal{A} \nu_0 D_\xi^*(\mathbf{R}_i) D_{-\xi}(\mathbf{R}_i) \mathbf{S} \cdot \mathbf{I}_i$. Even though both wave functions are highly oscillatory, this matrix element is generally finite. In other words, contact hyperfine interaction could potentially provide a valley-orbit coupling mechanism. We will qualitatively discuss this mechanism later in the manuscript.

The interface potential can also couple the two lowest-energy valleys, z and \bar{z} , if it is sufficiently sharp on the atomic length scale. These are represented by the term H_v in the Hamiltonian, which is a single-particle phenomenological coupling between the valleys in this study $\langle D_\xi | H_v | D_{-\xi} \rangle = \Delta$, with $\Delta > 0$. Δ is in principle complex (indeed it could be imaginary⁷⁰), yet here we assume it to be real for simplicity. The case of complex valley-orbit coupling will be discussed elsewhere.⁷⁹

We can now diagonalize the single-particle Hamiltonians with the valley-orbit coupling and obtain the *valley eigenstates* $D_\pm = (1/\sqrt{2})(D_z \pm D_{\bar{z}})$ with eigenvalues $\varepsilon_0 \pm \Delta$ in each of the quantum dots. Following Ref. [80], we then construct orthogonal single-dot wavefunctions (Wannier functions). Orthogonalizing L_ξ and R_ξ we obtain $\tilde{L}_\xi = \frac{L_\xi - g R_\xi}{\sqrt{1 - 2lg + g^2}}$ and $\tilde{R}_\xi = \frac{R_\xi - g L_\xi}{\sqrt{1 - 2lg + g^2}}$, where $g = (1 - \sqrt{1 - l^2})/l$, so that $\langle \tilde{R}_\xi | \tilde{L}_\xi \rangle = 0$. We define the matrix elements $\tilde{\varepsilon}_0 = \langle \tilde{D}_\xi | T + V_D | \tilde{D}_\xi \rangle$ and $\tilde{\Delta} = \langle \tilde{D}_\xi | H_v | \tilde{D}_{-\xi} \rangle$, as well as the matrix element for interdot tunneling $\tilde{t} = \langle \tilde{L}_\xi | H_0 | \tilde{R}_\xi \rangle + \langle \tilde{L}_\xi \tilde{L}_\xi | V_{ee} | \tilde{L}_\xi \tilde{R}_\xi \rangle$. We also orthogonalize the valley eigenstates L_\pm and R_\pm to obtain $\tilde{L}_\pm = \frac{L_\pm - g R_\pm}{\sqrt{1 - 2lg + g^2}}$ and $\tilde{R}_\pm = \frac{R_\pm - g L_\pm}{\sqrt{1 - 2lg + g^2}}$. It is straightforward to show that the four \tilde{D}_ξ form an orthogonal basis. These are the states we will use henceforth. All relevant matrix elements appearing throughout the text in what follows (t_0, s, k, j, u) are given in the Appendix. Now that we have obtained orthonormal single-electron eigenstates on each of the double dots (just the ground orbitals in each valley, assuming orbital excitation energy is large), we are ready to explore the low-energy two-spin spectrum of such a double dot in silicon and study the consequences of the multiple valleys.

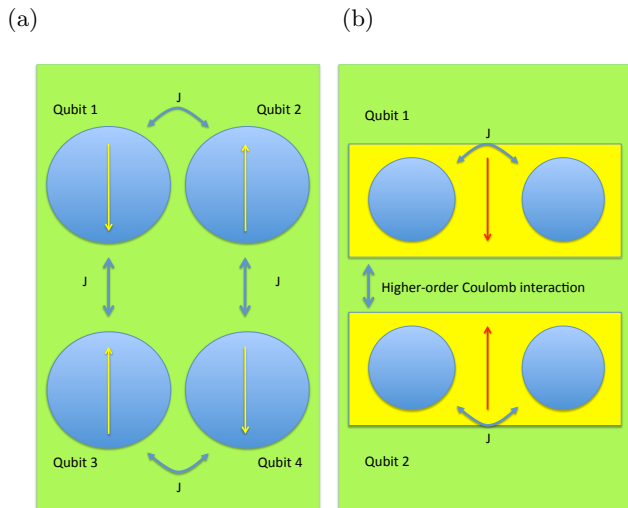


Figure 2: (color online) Spin-based quantum dot computer architectures. (a) Single-spin qubits (Loss-DiVincenzo architecture) employ a quantum dot array in which one electron spin is initialized in each dot. The arrows represent up and down spins. Single-qubit rotations are carried out using a magnetic field. Adjacent qubits are coupled by the exchange interaction, which is controlled by a tunable barrier. (b) Singlet-triplet qubits can be envisaged as an array of double quantum dots. In each DQD there are two electrons, which may be in a spin-singlet or a spin-triplet state. The up and down arrows represent spin triplets and singlets respectively. One-qubit rotations are accomplished via an inhomogeneous magnetic field. Two-qubit operations are described in Ref. 9.

III. SINGLE-SPIN QUBITS

For a single-spin qubit we first consider the initialization problem. In single-valley systems the lowest energy level in zero magnetic field is spin-degenerate but orbital-non-degenerate. Initialization of a definite single-spin state requires the application of a magnetic field so as to split the spin degeneracy via the Zeeman interaction, so that selective tunnelling from a reservoir can have high fidelity.¹⁴ Experimentally in GaAs this process requires magnetic fields of several Tesla brought about by the inherent smallness of the Bohr magneton, the small g -factor in GaAs ($|g| \sim 0.4$), and the constraint of ~ 100 mK electron temperature in the reservoir. In Si the g -factor is over four times larger ($g \sim 2$), so that at dilution refrigerator temperatures much smaller magnetic fields will be required than in GaAs, rendering spin initialization a relatively simple task. Nevertheless, there are now two possibly closely-spaced one-electron levels, for example \tilde{R}_+ and \tilde{R}_- , separated by the valley splitting Δ . As a result, initializing into a definite orbital state is dependent on the size of Δ , and may thus be problematic from the perspective of the requirement of two-spin exchange gates, as will be seen in what follows.

In the LDV architecture two-qubit gates are implemented by using the exchange interaction between neigh-

boring dots. Two-electron wave functions are generally superpositions of spin singlet and triplet states. A full singlet wave function comprises of a spatial and a spin part, $\Psi_S = \tilde{S}\chi_S$, where \tilde{S} is a two-particle spatially symmetric function and $|\chi_S\rangle$ is the two-spin singlet state given by $|\chi_S\rangle = (1/\sqrt{2})|\uparrow^{(1)}\downarrow^{(2)} - \downarrow^{(1)}\uparrow^{(2)}\rangle$. The superscript (i) denotes the i -th electron. Similarly full triplet wave functions are written as $\tilde{T}\chi_T$, where \tilde{T} is a two-particle spatially antisymmetric function and $|\chi_T\rangle$, representing the spin-triplet states, is an abbreviation which stands for $\chi_{\pm,0}$. The wave functions $|\chi_{\pm}\rangle$ represent the polarized spin triplets and are given by $|\uparrow^{(1)}\uparrow^{(2)}\rangle$ and $|\downarrow^{(1)}\downarrow^{(2)}\rangle$ respectively, while $|\chi_0\rangle$ represents the unpolarized spin triplet and has the form $|\chi_0\rangle = (1/\sqrt{2})|\uparrow^{(1)}\downarrow^{(2)} + \downarrow^{(1)}\uparrow^{(2)}\rangle$. In what follows we will frequently refer to just the spatially symmetric and antisymmetric states as the singlet and triplet states respectively, because the orbital part is where valleys play an important role.

Translating the Loss-DiVincenzo architecture to multi-valley systems requires taking into account the valley degree of freedom in the construction of many-particle wave functions. For a two-dot two-electron system, the spectrum is greatly expanded due to the presence of the additional orbital degree of freedom. In general, for a given number N of orbital states one can form $N(N+1)/2$ singlet and $3N(N-1)/2$ triplet two-electron states. In a single-valley system the number of orbital states is $N=1$, resulting in the trivial case of one singlet and three triplets. In a single Si QD we have $N=2$. For two electrons we now have $2(2+1)/2 = 3$ singlets and $3[2(2-1)]/2 = 3$ triplets. In a Si double dot $N=4$, so that there are $4(4+1)/2 = 10$ singlets and $3[4(4-1)]/2 = 18$ triplets. Therefore there are altogether 28 states for the double dot, of which 10 are spatially symmetric (spin singlets) and 18 are spatially antisymmetric (spin triplets). This number corresponds to the combination C_2^8 , where $8 \equiv 2^3$ arises as the product of a factor of 2 for the spin degree of freedom, a factor of 2 for the valley degree of freedom and a factor of 2 for the two dots. The combination C_2^8 is thus the number of combinations to construct a two-electron wave function out of 8 possible states, and represents the dimensionality of the representation of the permutation group on the combined two-dot two-spin two-valley $SU(2) \times SU(2) \times SU(2)$ Hilbert space.

These singlet and triplet states can be divided into three branches: states with the same valley composition, comprising wave functions of the form $(++)$ and $(--)$, and states with mixed valley composition, comprising wave functions of the form $(+-)$. There are thus in total *six* uncoupled branches, which can be labeled $(++)\tilde{S}$, $(+-)\tilde{S}$, $(--)\tilde{S}$ and $(++)\tilde{T}$, $(+-)\tilde{T}$, $(--)\tilde{T}$. For example, the spatial parts of the $++$ singlet and triplet states, arising from the higher-energy valley eigenstates,

are

$$\begin{aligned}
\tilde{S}_{++}^{LR} &= \frac{1}{\sqrt{2}} (\tilde{L}_+^{(1)} \tilde{R}_+^{(2)} + \tilde{L}_+^{(2)} \tilde{R}_+^{(1)}) \\
\tilde{S}_{++}^{RR} &= \tilde{R}_+^{(1)} \tilde{R}_+^{(2)} \\
\tilde{S}_{++}^{LL} &= \tilde{L}_+^{(1)} \tilde{L}_+^{(2)} \\
\tilde{T}_{++}^{LR} &= \frac{1}{\sqrt{2}} (\tilde{L}_+^{(1)} \tilde{R}_+^{(2)} - \tilde{L}_+^{(2)} \tilde{R}_+^{(1)})
\end{aligned} \tag{3}$$

The spatial parts of the $--$ singlet and triplet states, arising from the lower energy valley eigenstates, have similar constructions. For the $+-$ states, which have the two electrons in different valleys, we list the singlets and the triplets separately. The spatial parts of the singlet states are

$$\begin{aligned}
\tilde{S}_{+-}^{LR} &= \frac{1}{\sqrt{2}} (\tilde{L}_+^{(1)} \tilde{R}_-^{(2)} + \tilde{L}_+^{(2)} \tilde{R}_-^{(1)}) \\
\tilde{S}_{-+}^{LR} &= \frac{1}{\sqrt{2}} (\tilde{L}_-^{(1)} \tilde{R}_+^{(2)} + \tilde{L}_-^{(2)} \tilde{R}_+^{(1)}) \\
\tilde{S}_{+-}^{RR} &= \frac{1}{\sqrt{2}} (\tilde{R}_+^{(1)} \tilde{R}_-^{(2)} + \tilde{R}_+^{(2)} \tilde{R}_-^{(1)}) \\
\tilde{S}_{-+}^{LL} &= \frac{1}{\sqrt{2}} (\tilde{L}_+^{(1)} \tilde{L}_-^{(2)} + \tilde{L}_+^{(2)} \tilde{L}_-^{(1)}),
\end{aligned} \tag{4}$$

while the spatial parts of the triplet states are

$$\begin{aligned}
\tilde{T}_{+-}^{LR} &= \frac{1}{\sqrt{2}} (\tilde{L}_+^{(1)} \tilde{R}_-^{(2)} - \tilde{L}_+^{(2)} \tilde{R}_-^{(1)}) \\
\tilde{T}_{-+}^{LR} &= \frac{1}{\sqrt{2}} (\tilde{L}_-^{(1)} \tilde{R}_+^{(2)} - \tilde{L}_-^{(2)} \tilde{R}_+^{(1)}) \\
\tilde{T}_{+-}^{RR} &= \frac{1}{\sqrt{2}} (\tilde{R}_+^{(1)} \tilde{R}_-^{(2)} - \tilde{R}_+^{(2)} \tilde{R}_-^{(1)}) \\
\tilde{T}_{-+}^{LL} &= \frac{1}{\sqrt{2}} (\tilde{L}_+^{(1)} \tilde{L}_-^{(2)} - \tilde{L}_+^{(2)} \tilde{L}_-^{(1)}).
\end{aligned} \tag{5}$$

The spatially symmetric functions \tilde{S} split into three single-valley states from the lower-energy $--$ branch, three single-valley states from the higher-energy $++$ branch, and four states from the $+-$ branch. The spatially antisymmetric functions \tilde{T} split into one single-valley state from the lower-energy $--$ branch, another single-valley state from the higher-energy $++$ branch and four states from the $+-$ branch. As we discussed before, the smooth quantum dot confinement potential and the electron-electron Coulomb interaction do not introduce further transitions between valleys (the matrix elements are mostly exponentially suppressed, and the only Coulomb matrix element that is not exponentially suppressed is nonetheless very small, as we show in the Appendix). Thus the $--$, $++$ and $+-$ branches do not mix, allowing us to analyze them separately by writing out the matrix elements of the DQD Hamiltonian in each branch.

The two-electron Hamiltonian in the $++$ branch has the form

$$H_{++} = 2\tilde{\epsilon}_0 + 2\tilde{\Delta} + \begin{pmatrix} \tilde{k} + \tilde{j} & \tilde{t}\sqrt{2} & \tilde{t}\sqrt{2} & 0 \\ \tilde{t}\sqrt{2} & \tilde{u} & \tilde{j} & 0 \\ \tilde{t}\sqrt{2} & \tilde{j} & \tilde{u} & 0 \\ 0 & 0 & 0 & \tilde{k} - \tilde{j} \end{pmatrix}. \tag{6}$$

Al the matrix elements are given in the Appendix. The Hamiltonian H_{--} in the $--$ branch takes the same form, with exactly the same matrix elements, except $2\tilde{\Delta} \rightarrow -2\tilde{\Delta}$. In other words, $H_{--} = H_{++} - 4\tilde{\Delta}$. This equality is determined by the fact that the two dots have the same valley splitting, and the valley eigenstates have the same composition.

In the $+-$ singlet branch, since the overlap between states from different valleys is negligible, matrix elements of the form $\langle \tilde{S}_{+-} | H_0 | \tilde{S}_{+-} \rangle$ and $\langle \tilde{T}_{+-} | H_0 | \tilde{T}_{+-} \rangle$ are equal. Thus the Hamiltonian takes the form

$$H_{+-}^S = 2\tilde{\epsilon}_0 + \begin{pmatrix} \tilde{k} & \tilde{j} & \tilde{t} & \tilde{t} \\ \tilde{j} & \tilde{k} & \tilde{t} & \tilde{t} \\ \tilde{t} & \tilde{t} & \tilde{u} & \tilde{j} \\ \tilde{t} & \tilde{t} & \tilde{j} & \tilde{u} \end{pmatrix}. \tag{7}$$

The Hamiltonian in the $+-$ triplet branch H_{+-}^T takes the same form, with the same matrix elements up to a sign difference. It turns out that the eigenvalues of states in the triplet branch are exactly the same as those in the singlet branch, thus the singlet and triplet $+-$ branches are degenerate. We will not write down H_{+-}^T explicitly.

The structure of the Hamiltonian has important consequences for the operation of spin qubits in silicon. The $++$ and $--$ branches have the same structure as the single-valley Hamiltonian except they are shifted up and down by $2\tilde{\Delta}$ respectively. These branches can be regarded as replicas of the usual single-valley Hund-Mulliken Hamiltonian.^{80,81} The singlet and triplet states have the same form as in the single-valley case. The principal difference from the one-valley situation emerges when we consider the $+-$ branches, where we have four sets of degenerate singlet and triplet states. This degeneracy is the direct manifestation of the fact that exchange integrals for electrons from different valleys vanish (either exponentially small or very small due to Bloch function symmetry, see Appendix).

The essence of the exchange gates in the Loss-DiVincenzo architecture is the control of the phase difference (introduced by a finite exchange splitting) between singlet and triplet states. In the $--$ or $++$ branches the two electrons are in the same valley eigenstate, so that we exactly recover the single-valley physics of GaAs, and exchange gates can be implemented. However, in the $+-$ and $-+$ branches singlet and triplet states are degenerate, rendering exchange gates impossible. Now assume that the two electrons were initialized into the two initially independent quantum dots with an arbitrary combination of valley eigenstates. When the inter-dot barrier is lowered, the two-electron states would generally populate all four branches ($++$, $+-$, $-+$, and $--$). Since exchange gates cannot be implemented in the $+-$ and $-+$ branches, they cannot be implemented for these two electrons in general. The only way to perform exchange gates is to have the two-electron states populating only the $++$ and $--$ branches. With the electrons in a reservoir in a structure-less Fermi distribution, the only single-electron

state that can be loaded exclusively is the $-$ valley eigenstate (if $2\tilde{\Delta} \gg k_B T$), so that when inter-dot tunnelling is turned on, the two electrons are in the $--$ branch. This is the only viable option where exchange gates can still be performed. The exchange splitting between the lowest-lying singlet and triplet states in the $--$ branch is given by the Hund-Mulliken expression,^{80,82} which can be obtained by straightforward diagonalization of Eq. (6),

$$J = -2\tilde{j} - \frac{(\tilde{u} - \tilde{k})}{2} + \frac{1}{2} \sqrt{(\tilde{u} - \tilde{k})^2 + 16\tilde{t}^2}. \quad (8)$$

The graph of exchange versus interdot separation has the same form as in the single-valley case.^{80,82} Based on the analysis presented above, it is natural to conclude that the optimal strategy for single-spin qubits in multi-valley DQDs is to strive to obtain a large valley splitting and work towards replicating the single-valley situation.

The case of large valley splitting has been analyzed thoroughly in a recent publication.⁸² It was demonstrated that in this situation single-spin qubits can be implemented, provided that experimental design takes into consideration the significantly different values of parameters in Si as compared to GaAs. For example, the carrier effective mass in Si is approximately three times larger than in GaAs, resulting in a requirement of tighter confinement in order to achieve the same orbital level splitting. Furthermore, in a MOSFET, the Coulomb interaction between electrons is enhanced by the image charge in the substrate, which has a much smaller dielectric constant (this is not the case in Si/SiGe), thus shrinking the regime of applicability of simple analytical methods of calculating the exchange splitting (i.e. the Hund-Mulliken method). However, these issues, while posing both experimental and calculational problems, are rather technical difficulties, and in principle, if the valley splitting is large $2\tilde{\Delta} \gg k_B T$, the valley degree of freedom does not present a fundamental obstacle to the implementation of single-spin qubits.

IV. SINGLET-TRIPLET QUBITS

In the setup employed for the implementation of singlet-triplet qubits we choose the external electric field $E > 0$, so that the energy of the left dot is raised with respect to the right dot. We use the notation (n, m) to indicate the occupancy of the left and right dots respectively. A finite electric field is required in order to drive the system close to the avoided crossing of the (0,2) and (1,1) singlet states, which allows high-fidelity initialization in the (0,2) regime, and manipulation of the two-spin states using an inhomogeneous magnetic field and exchange splitting in the (1,1) regime. In this architecture single-particle energies on the left and right dots are different, therefore we define the energies $\tilde{\epsilon}_R = \langle \tilde{R}_\xi | (T + V_Q) | \tilde{R}_\xi \rangle$ and $\tilde{\epsilon}_L = \langle \tilde{L}_\xi | (T + V_Q) | \tilde{L}_\xi \rangle$, the dimensionless detuning as $\delta = (\tilde{\epsilon}_L - \tilde{\epsilon}_R) / (2d\tilde{\epsilon}_0)$, and the dimensionless critical detuning $\delta_c = (\tilde{u} - \tilde{k}) / (2d\tilde{\epsilon}_0)$.

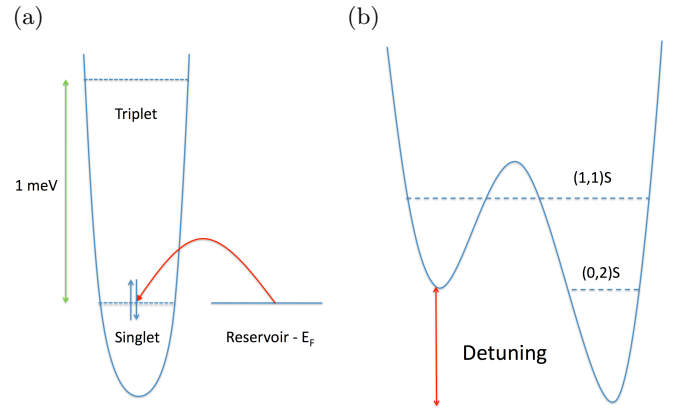


Figure 3: (color online) Initialization of a singlet-triplet qubit in a single-valley system. (a) The detuning on the left dot is raised and only the right dot needs to be considered. An outside reservoir at energy E_F is aligned with the lowest two-electron energy level, which is a singlet. Two electrons then tunnel onto the right dot into the (0,2) singlet state. The (0,2) triplet state is separated by an energy on the order of the confinement energy, which in GaAs is on the order of 1 meV, and is expected to be comparable in Si. (b) The detuning is lowered until the (1,1) singlet state is at the same energy as the (0,2) singlet state. At this point an electron will tunnel from the right dot onto the left dot.

Our study of the singlet-triplet qubit follows the successful experimental implementation in GaAs DQDs.² In this particular approach a (0,2) singlet state is at first initialized, as shown in Fig. 3(b). The double dot is then pushed deep into the (1,1) regime. A uniform magnetic field is used to split off the polarized triplet states. Since the tunnel coupling between the dots is small the singlet and unpolarized triplet levels are practically degenerate. In GaAs QDs the small and random inhomogeneous nuclear magnetic field can then rotate the two-electron states between the singlet and the unpolarized triplet states. After some mixing time in the (1,1) regime, tuning the bias returns the system to the (0,2) configuration, where electrical readout is accomplished using spin blockade.¹⁷ The procedure is repeated many times (essentially an ensemble average in the time domain) and the probability that the system returns to the (0,2) singlet state is determined.²³ This scheme has very reliable initialization, and in GaAs the intrinsic nuclear fields lead to rich physics. The double dot architecture also allows good spin-charge conversion so that measurement fidelity can be rather good, and single-shot measurement using the Radio-Frequency Quantum Point Contact (RF-QPC) or Radio-Frequency Single-electron transistor (RF-SET).²¹

Below we investigate the implications of the existence of the valley degree of freedom for a quantum coherent experiment on singlet-triplet qubits in Si of the kind described above. In particular we focus on the two-electron single-dot spectrum to describe the initialization process, and on the two-electron double-dot spectrum to explore

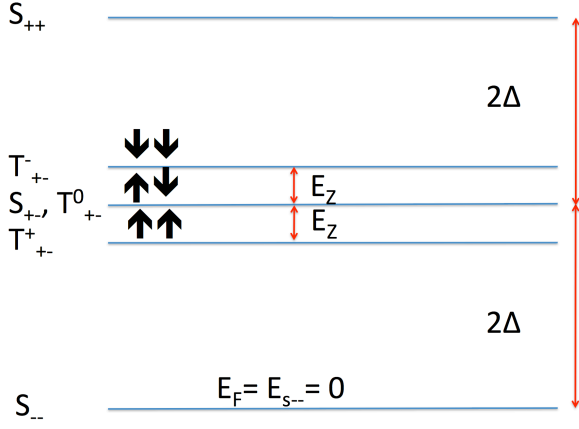


Figure 4: Two-electron energy levels on a single dot at finite Δ and magnetic field such that $2\Delta > E_Z$. In this case the lowest energy state is the singlet S_{--} , followed by the triplet T_{+-}^+ , the degenerate singlet S_{+-} /triplet T_{+-}^0 and triplet T_{+-}^- , and finally the singlet S_{++} . The spin orientations of the electrons in triplet states are indicated by arrows.

the operations of the qubit.

A. Single-dot spectrum

We first consider the single-dot two-electron spectrum and the initialization process. Specifically, we examine the spectrum of a doubly occupied right dot. Using the notation of Sec. III, the four lowest-energy two-particle spatial wave functions are,

$$\begin{aligned}\tilde{S}_{--}^{RR} &= \tilde{R}_-^{(1)} \tilde{R}_-^{(2)} \\ \tilde{S}_{++}^{RR} &= \tilde{R}_+^{(1)} \tilde{R}_+^{(2)} \\ \tilde{S}_{+-}^{RR} &= (1/\sqrt{2})(\tilde{R}_+^{(1)} \tilde{R}_-^{(2)} + \tilde{R}_+^{(2)} \tilde{R}_-^{(1)}) \\ \tilde{T}_{+-}^{RR} &= (1/\sqrt{2})(\tilde{R}_+^{(1)} \tilde{R}_-^{(2)} - \tilde{R}_+^{(2)} \tilde{R}_-^{(1)}),\end{aligned}\quad (9)$$

In the basis spanned by $\{\tilde{S}_{--}^{RR}, \tilde{S}_{+-}^{RR}, \tilde{T}_{+-}^{RR}, \tilde{S}_{++}^{RR}\}$ the Hamiltonian is

$$H_{1dot} = 2\tilde{\varepsilon}_0 + \tilde{u} + \begin{pmatrix} -2\tilde{\Delta} & 0 & 0 & 0 \\ 0 & 0 & 0 & 0 \\ 0 & 0 & 0 & 0 \\ 0 & 0 & 0 & 2\tilde{\Delta} \end{pmatrix}. \quad (10)$$

Notice here that the four basis states are still eigenstates because the smooth double dot potential and the Coulomb interaction do not mix the valleys. The on-site Coulomb matrix element $\tilde{u} = \int d^3r_1 \int d^3r_2 |\tilde{R}_{z,\bar{z}}^{(1)}|^2 V_{ee} |\tilde{R}_{z,\bar{z}}^{(2)}|^2$ involves the charge densities from the two valleys. In the evaluation of Eq. (10) we have also encountered a *valley-exchange* Coulomb integral

$$j_v = \int d^3r_1 \int d^3r_2 \tilde{R}_z^{*(1)} \tilde{R}_{\bar{z}}^{*(2)} V_{ee} \tilde{R}_{\bar{z}}^{(1)} \tilde{R}_z^{(2)}. \quad (11)$$

Unlike all other terms involving the overlap of states between different valleys this integral is not suppressed by an exponentially small prefactor. However, we find its value to be $\ll 1\mu\text{eV}$ and we thus do not take it into account in our analysis. The numerical evaluation of this term is discussed in Appendix D.

From Eq. (10) it is evident that, for $\tilde{\Delta} = 0$ and no external magnetic field \mathbf{B} , all six lowest-energy levels are degenerate. Under these circumstances it is not possible to load any particular two-electron state. If an external magnetic field is applied the triplet energy levels are split by the Zeeman energy E_Z . We have shown in Fig. 4 the spectrum for finite valley coupling $\tilde{\Delta}$ and magnetic field \mathbf{B} for the case when $2\tilde{\Delta} > E_Z$. First the states are split by $2\tilde{\Delta}$ as can be seen from Eq. (10). The triplet states also split into T_{+-}^+ , T_{+-}^0 , and T_{+-}^- , separated in energy by E_Z , leaving only the singlet S_{+-} and the unpolarized triplet T_{+-}^0 as two degenerate states which cannot be further split.

Initialization of a (0,2) state in the quantum dot requires an outside reservoir, with a Fermi energy ε_F , which is thermally broadened by $\approx k_B T$. The reservoir is tuned to be on resonance with the lowest-energy singlet state. If we assume the tunnel couplings between all QD states and the reservoir to be identical the probability of loading a certain state is proportional to the Fermi distribution at the energy of this state. In the optimal case in which $\tilde{\Delta} \gg k_B T$ the lowest-energy singlet state \tilde{S}_{--}^{RR} can be loaded exclusively. Therefore the condition $\tilde{\Delta} \gg k_B T$ constitutes the first requirement in the operational definition of a qubit in Si-based QDs. At dilution refrigerator temperatures of $T=100\text{mK}$ we have $k_B T \approx 0.01\text{meV}$. Under these circumstances $\tilde{\Delta} \approx 0.1\text{meV}$ is sufficient to ensure the lowest-energy singlet state can be initialized unambiguously. In this regime the two-electron initialization process in a Si DQD is identical to the GaAs DQD in Ref. 2 and is an effective single-valley problem.

The qubit of Refs. 2,17 is made in a single-valley system, so $\tilde{R}_\pm \rightarrow \tilde{R}$. The only two-particle state that can be made out of the lowest lying wave function is a singlet. There is no low-energy triplet, since the triplet must involve higher orbitals, so it is separated by an energy of the order of the single-particle confinement energy ε_0 , which is on the order of meV, minus a small exchange term. Therefore in GaAs the qubit can be straightforwardly initialized. In Si, if $\tilde{\Delta}$ is sufficiently large the two-electron two-valley single-dot problem effectively becomes a single-valley problem. But the energy scale in this case is set by $\tilde{\Delta}$, which in general could be considerably less than the confinement energy.

B. Double-dot spectrum

Single-qubit operations in the singlet-triplet qubit is performed in the (1,1) regime.² The two-particle states are the same as those enumerated in the case of single-spin qubits except here we do not include the high-energy

(2,0) states of the form $\tilde{L}\tilde{L}$. In our basis there are thus seven spatially symmetric Hund-Mulliken (HM) wave functions (four (1,1) states and three (0,2) states) of the lowest-energy two-spin singlet states. As in the LDV architecture, these singlet states belong to three uncoupled branches. These are \tilde{S}_{++}^{LR} and \tilde{S}_{++}^{RR} from the lower-energy valley eigenstates, \tilde{S}_{++}^{LR} and \tilde{S}_{++}^{RR} from the higher-energy valley eigenstates, and \tilde{S}_{+-}^{LR} , \tilde{S}_{+-}^{LR} and \tilde{S}_{+-}^{RR} valley-mixing states. There are also five spatially antisymmetric states, in turn split into three branches: $\{\tilde{T}_{++}^{LR}\}$ and $\{\tilde{T}_{--}^{LR}\}$ are the HM spatially antisymmetric states each composed of a single valley eigenstate, while $\{\tilde{T}_{+-}^{LR}, \tilde{T}_{+-}^{LR}, \tilde{T}_{+-}^{RR}\}$ are mixed-valley spatially antisymmetric states.

We proceed exactly as in the case of the single-spin qubit, determining the matrix elements of the Hamiltonian in each of the six independent branches with different spin and valley character. In the basis $\{\tilde{S}_{++}^{LR}, \tilde{S}_{++}^{RR}, \tilde{T}_{++}^{LR}\}$ the matrix elements of the Hamiltonian in the $++$ branch are given by

$$H_{++} = \tilde{\varepsilon}_L + \tilde{\varepsilon}_R + \tilde{k} + 2\tilde{\Delta} + \begin{pmatrix} \tilde{j} & \tilde{t}\sqrt{2} & 0 \\ \tilde{t}\sqrt{2} & -2d\varepsilon_0(\delta - \delta_c) & 0 \\ 0 & 0 & -\tilde{j} \end{pmatrix}. \quad (12)$$

As before, the matrix elements in the $--$ branch are the same except $2\tilde{\Delta} \rightarrow -2\tilde{\Delta}$. The matrix elements in the $+-$ singlet branch, in the basis $\{\tilde{S}_{+-}^{LR}, \tilde{S}_{+-}^{LR}, \tilde{S}_{+-}^{RR}\}$, are

$$H_{+-}^S = \tilde{\varepsilon}_L + \tilde{\varepsilon}_R + \tilde{k} + \begin{pmatrix} 0 & \tilde{j} & \tilde{t} \\ \tilde{j} & 0 & \tilde{t} \\ \tilde{t} & \tilde{t} & -2d\varepsilon_0(\delta - \delta_c) \end{pmatrix}. \quad (13)$$

The matrix elements of the Hamiltonian in the $+-$ triplet branch have the same magnitude as the matrix elements in the $+-$ singlet branch, yet some differ in sign. In the basis $\{\tilde{T}_{+-}^{LR}, \tilde{T}_{+-}^{LR}, \tilde{T}_{+-}^{RR}\}$

$$H_{+-}^T = \tilde{\varepsilon}_L + \tilde{\varepsilon}_R + \tilde{k} + \begin{pmatrix} 0 & -\tilde{j} & \tilde{t} \\ -\tilde{j} & 0 & -\tilde{t} \\ \tilde{t} & -\tilde{t} & -2d\varepsilon_0(\delta - \delta_c) \end{pmatrix}. \quad (14)$$

The sign difference in the tunneling matrix elements has important consequences for spin blockade, which will be examined below.

The $+-$ singlet and triplet branches always yield the same energies. Moreover, for $\tilde{\Delta} = 0$ some of the eigenvalues of the $+-$ singlet and triplet branch also coincide with eigenvalues of the $++$ and $--$ singlet and triplet branches. As a consequence of this, for $\tilde{\Delta} = 0$ the lowest energy state is a degenerate singlet/triplet. On the other hand, when the two electrons are in the same valley, the singlet and triplet have different energies because of the exchange term \tilde{j} .

For clarity we focus on a concrete example, taking a Si DQD with $a=8.2\text{nm}$, $b=3\text{nm}$, $d=2.45$ and $\tilde{\Delta}=0.1\text{meV}$. The energy levels of the system with these parameters are plotted in Fig. 5 as a function of the dimensionless detuning δ . At low detuning there are four (0,2) high-energy levels, indicated by the two solid lines (representing singlets of the form $\tilde{R}_+\tilde{R}_+$, $\tilde{R}_-\tilde{R}_-$) and one dashed

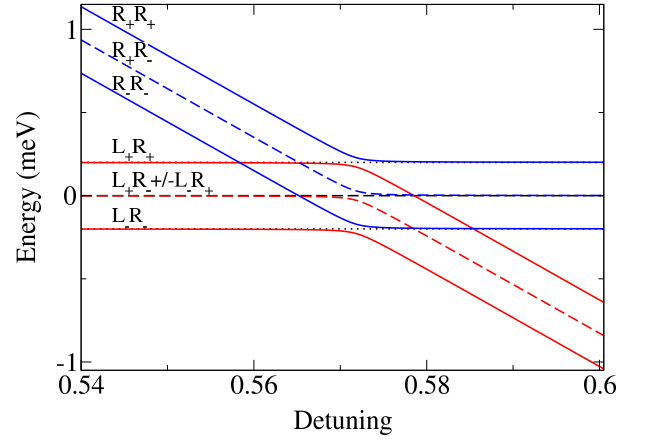


Figure 5: DQD spectrum for a Si/SiO₂ DQD with $a=8.2\text{nm}$, $b=3\text{nm}$, $d=2.45$, $\tilde{t} = 0.02\text{meV}$, $\tilde{\Delta}=0.1\text{meV}$ and zero magnetic field. The top and bottom anticrossings each consist of two singlets (solid lines) and one triplet (dotted line). In the middle anticrossing each of the three dashed lines represents a degenerate singlet/triplet level.

line (representing two degenerate singlet and triplet of the form $\tilde{R}_+\tilde{R}_-$). The separation of these levels is $2\tilde{\Delta}$. There are also eight lower-energy (1,1) levels: a degenerate singlet/triplet of the form $\tilde{L}_+\tilde{R}_+$ (top solid line), a degenerate singlet/triplet of the form $\tilde{L}_-\tilde{R}_-$ (bottom solid line), and two degenerate valley mixing singlets and triplets of the form $\tilde{L}_+\tilde{R}_-$ and $\tilde{L}_-\tilde{R}_+$. For the parameters considered in this example, using the method described in Appendix C, we have calculated $\tilde{t} \approx 0.02\text{meV}$, giving a splitting at the avoided crossing of $\approx 0.06\text{meV}$.

C. Double dot spectra in different parameter regimes

Up to now we have considered the simplest form of the two-dot spectrum, which occurs in the case when $\tilde{\Delta}$ is the largest energy scale, exceeding the tunnel coupling and the Zeeman splitting due to the uniform magnetic field by a noticeable amount. Yet it is evident that the qualitative features of the spectrum are sensitively dependent on the relative size of \tilde{t} , $\tilde{\Delta}$, and E_Z . As these parameters vary with respect to one another, the relative position of most energy levels can differ greatly. As a result, there can be substantial variation in the loading and mixing dynamics of the two-electron states, and Figs. 6–10 are intended to illustrate this fact.

In Fig. 5 we plot the two-electron spectrum of a Si DQD when $\tilde{\Delta} \gg \tilde{t}$ without showing the multitude of Zeeman-split levels for ease of explanation of its essential physical features. To compensate for this in Fig. 6 we have shown the same spectrum but included *all* the Zeeman-split levels, while continuing to assume that $\tilde{\Delta} \gg \tilde{t}$. It is interesting to follow the evolution of the two-dot two-electron spectrum as the ratio of the mag-

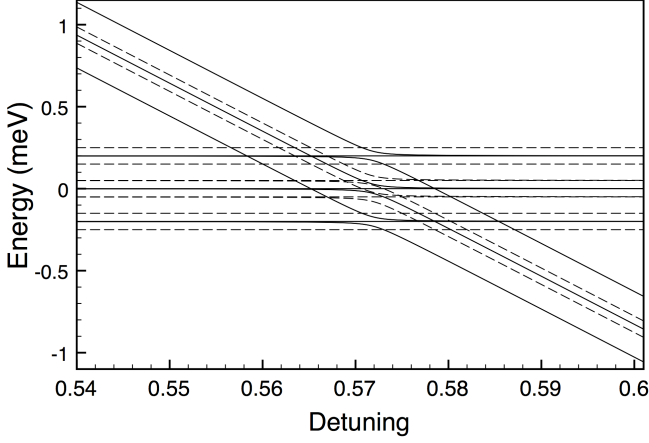


Figure 6: Energy level spectrum for a Si/SiO₂ DQD with $a=8.2\text{nm}$, $b=3\text{nm}$, $d=2.45$ and $\tilde{\Delta}=0.1\text{meV}$, $E_Z = 0.05\text{ meV}$, $\tilde{t}=0.02\text{meV}$. In this figure we have plotted the same energy levels as in Fig. 5, except that the polarized triplet states are shown explicitly in a uniform magnetic field. The solid lines represent singlet and unpolarized triplet levels \tilde{S} and \tilde{T}^0 , while the dashed lines represent polarized triplet levels \tilde{T}^+ and \tilde{T}^- .

netic field to the valley splitting goes from small to large. This can be done by observing the way the spectrum changes from Figs. 6 through 9. These figures taken together illustrate the fact that, as the magnetic field increases with respect to the valley coupling there is a transition between the valley physics (which is in effect a pseudospin) and the Zeeman physics (which is due to the real spin). For large valley/Zeeman splitting the spectrum looks effectively the same, except in one extreme case the splitting between the three sets of levels is determined by $\tilde{\Delta}$ whereas in the other extreme case it is determined by E_Z .

On the other hand Fig. 10 contains the two-dot spectrum for the opposite case when $\tilde{\Delta} \ll \tilde{t}$. In Figs. 6 and 10 we have assumed the same value of the Zeeman splitting. Finally, in general case one should be prepared for an intermediate scenario as in Fig. 8 in which the sets of levels are not clearly separated and may cross. In such a situation distinguishing the energy levels experimentally may prove challenging.

D. Inhomogeneous magnetic fields in Si

Quantum coherent experiments on singlet-triplet qubits make use of an inhomogeneous magnetic field. As shown in Ref. 2, an experiment on the singlet-triplet qubit often requires two magnetic fields: a uniform one to separate out the polarized triplet states, and an inhomogeneous one to mix the singlet and the unpolarized triplet states. In GaAs the latter is provided by the lattice nuclear spins. In Si, hyperfine interaction is much weaker, and number of lattice nuclear spins much

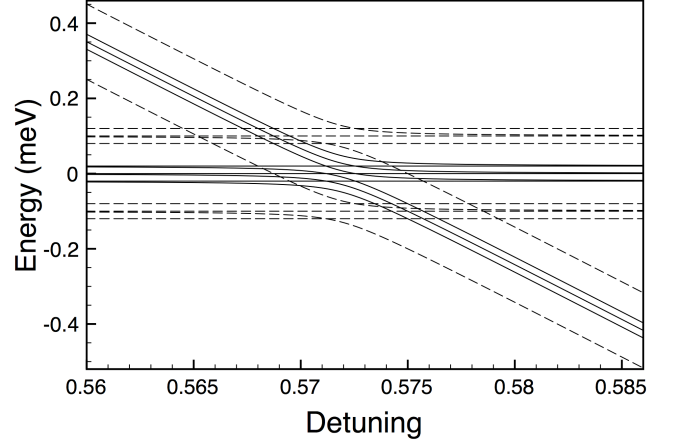


Figure 7: Energy level spectrum for a Si/SiO₂ DQD with $a=8.2\text{nm}$, $b=3\text{nm}$, $d=2.45$ and $\tilde{\Delta}=0.01\text{meV}$, $E_Z = 0.1\text{ meV}$, $\tilde{t}=0.02\text{meV}$. Here the valley splitting $\tilde{\Delta}$ has been set as the smallest energy scale, the Zeeman energy as the largest scale, and the tunnel coupling in between. This figure illustrates the opposite scenario to Fig. 6, showing the qualitatively different structure of the energy spectrum when $\tilde{\Delta} < \tilde{t}$.

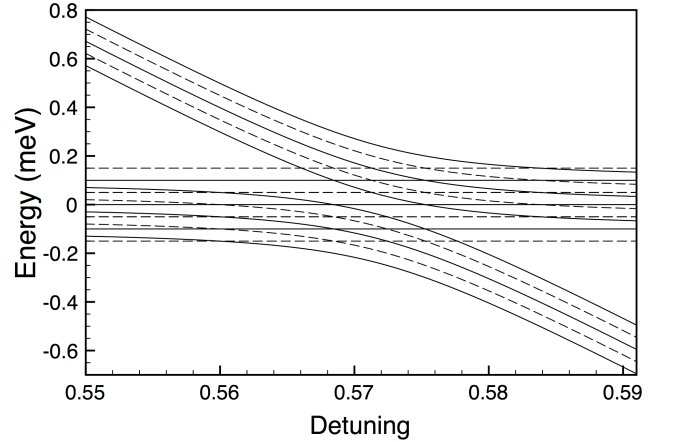


Figure 8: Energy level spectrum for a Si/SiO₂ DQD with $a=8.2\text{nm}$, $b=3\text{nm}$, $d=2.45$ and $\tilde{\Delta}=0.05\text{meV}$, $E_Z = 0.05\text{ meV}$, $\tilde{t}=0.1\text{meV}$. In this figure the tunnel coupling has been set as the largest energy scale. Although the magnitude of \tilde{t} in this graph has been exaggerated for clarity and exceeds what one expects to measure experimentally, this figure illustrates the complications inherent in experiments seeking to distinguish parameters of comparable magnitude.

smaller. Natural Si has only 4.7% of the ²⁹Si isotope having nonzero nuclear spin (²⁸Si has no nuclear spin) and it can be further isotopically purified to nearly completely eliminate the nuclear spins. In case of inhomogeneous effective field coming from hyperfine interaction with the nuclei in the dots, the magnetic fields on the left and right dots (\mathbf{B}_L and \mathbf{B}_R below) differ by a small amount of the order of \mathcal{A}/\sqrt{N} where \mathcal{A} is the hyperfine constant of the material and N is the number of nuclei interacting

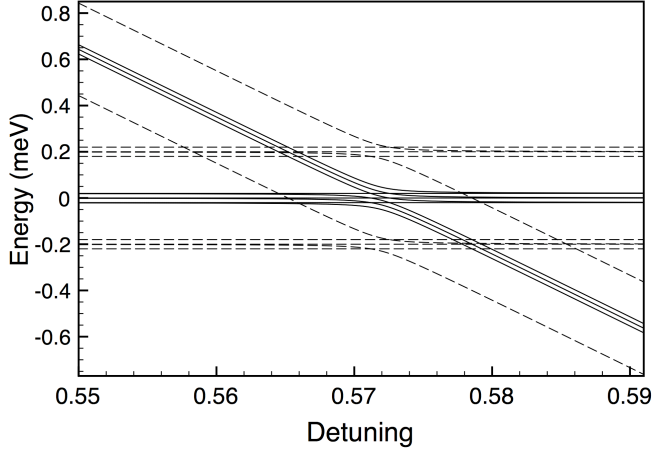


Figure 9: Energy level spectrum for a Si/SiO₂ DQD with $a=8.2\text{nm}$, $b=3\text{nm}$, $d=2.45$ and $\tilde{\Delta}=0.01\text{meV}$, $E_Z = 0.2\text{ meV}$, $\tilde{t}=0.02\text{meV}$. In this figure the Zeeman energy has been set as the largest energy scale and the valley splitting as the lowest. Notice the qualitative similarity of this figure to Fig. 6. As the magnetic field increases, in effect the Zeeman field and the valley-orbit coupling trade places.

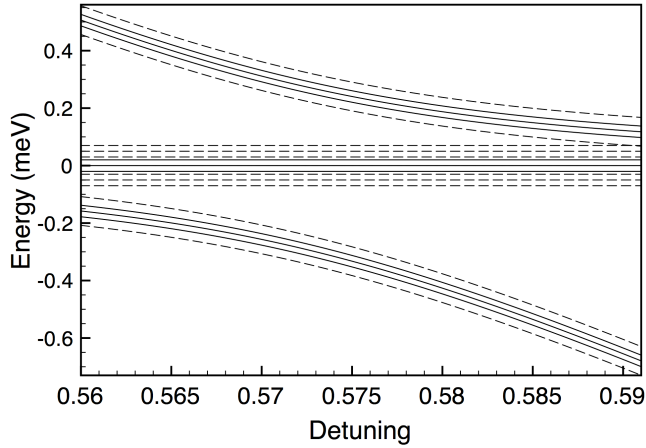


Figure 10: Energy level spectrum for a Si/SiO₂ DQD with $a=8.2\text{nm}$, $b=3\text{nm}$, $d=2.45$ and $\tilde{\Delta}=0.01\text{meV}$, $E_Z = 0.05\text{ meV}$, $\tilde{t}=0.2\text{meV}$. This figure illustrates the case when the tunnel coupling is the largest energy scale in the problem.

appreciably with the electrons. In gated GaAs QDs this amount is on the order of mT. In a Si QD it has been estimated to be in the range 1-3 neV, corresponding to a time scale of 0.3-1 μs and magnetic fields of tens of μT .⁴² In future systems based on purified Si, an external inhomogeneous magnetic field must be generated by other means, such as the use of a nanomagnet. In fact, a nanomagnet could potentially allow for better control. For example, one can tailor the inhomogeneous field to have only a \hat{z} -component.

Each initialized (0,2) state has a probability of return to the original state after staying for a certain time in the

(1,1) regime. In a random hyperfine field this probability of return is determined by the nuclear spin polarization difference between the two dots. Since the experiment is repeated many times in the time domain, the observed results involve averages over the inhomogeneous nuclear field. On the other hand, in an applied inhomogeneous magnetic field, the field is the same during each experimental run. Therefore, by controlling the magnitude and orientation of the applied inhomogeneous field one can control the composition of the (1,1) state after mixing, and therefore the return probability. In this case we thus have a controlled return probability. The key fact is that, in the far-detuned (1,1) regime where $\delta \ll \delta_c$, each unpolarized state (singlet or triplet) mixes with one other unpolarized state, while polarized triplets do not mix with any other state (see Sec. IV E). It should be pointed out that knowledge of the controlled return probability does require exact knowledge and control of the applied inhomogeneous magnetic field inside each dot.

E. Singlet-triplet mixing in an inhomogeneous magnetic field

While tuning an applied electric field leads to a change in the orbital state of the double dot, an inhomogeneous magnetic field induces coupling between singlet and triplet states. We will refer explicitly to the spin wave functions, and will write the full two-electron wave function as, e.g., $\Psi_{S,++}^{LR} = \tilde{S}_{++}^{LR}\chi_S$ as explained above.

We consider a general inhomogeneous magnetic field, which is the sum of the nuclear field plus the applied field $\mathbf{B}(\mathbf{r}) = \mathbf{B}_{nuc}(\mathbf{r}) + \mathbf{B}_{appl}(\mathbf{r})$. The Zeeman Hamiltonian in Si, where $g = 2$ approximately, is simply $-\mu_B \boldsymbol{\sigma} \cdot \mathbf{B}$. For two electrons in a DQD we have a position-dependent Zeeman Hamiltonian composed of two terms

$$H_Z = -\mu_B [\boldsymbol{\sigma}_1 \cdot \mathbf{B}(\mathbf{r}_1) + \boldsymbol{\sigma}_2 \cdot \mathbf{B}(\mathbf{r}_2)] \quad (15)$$

where the spin operators $\boldsymbol{\sigma}_{1,2}$ act on the spin of particle 1 and 2 respectively.

The expectation values of the Zeeman Hamiltonian contain expressions of the form

$$\begin{aligned} \langle \tilde{L}_{\pm}^{(1)} | \mathbf{B}(\mathbf{r}_1) | \tilde{L}_{\pm}^{(1)} \rangle &= \mathbf{B}_L \\ \langle \tilde{R}_{\pm}^{(1)} | \mathbf{B}(\mathbf{r}_1) | \tilde{R}_{\pm}^{(1)} \rangle &= \mathbf{B}_R \\ \langle \tilde{L}_{\pm}^{(1)} | \mathbf{B}(\mathbf{r}_1) | \tilde{R}_{\pm}^{(1)} \rangle &\approx 0. \end{aligned} \quad (16)$$

We write these (real or effective) magnetic fields in the form $\mathbf{B}_{L,R} = (\mathbf{B}_{tot} \pm \Delta\mathbf{B})/2$, where the total magnetic field is $\mathbf{B}_{tot} = \mathbf{B}_L + \mathbf{B}_R$ and the field difference is $\Delta\mathbf{B} = \mathbf{B}_L - \mathbf{B}_R$.

For the case of an applied magnetic field the Zeeman Hamiltonian does not mix states from different valleys. This is because experimentally one cannot generate an applied field with profile sufficiently sharp in the

\hat{z} -direction to mix states from different valleys, which have very different wavevectors. Within the mixed-valley branch, neither an applied field nor the nuclear field can mix $+-$ states with $-+$ states at the mean field limit. Hyperfine interaction does mix states from different branches because contact hyperfine interaction is sharply local in space (δ function in space) so that it has finite transition matrix element between different electronic valleys. Valley mixing due to the inhomogeneous nuclear field is addressed in Sec. IV G. In what follows here we only consider the matrix elements of the Zeeman Hamiltonian within each branch of the two-dot spectrum, i.e. $++$, $--$ and $+-$.

Mixing of the singlet and triplet states occurs in the (1,1) configuration, when $\delta \ll \delta_c$. Therefore, without putting in valley eigenstate indices, we are interested in the effect of the Zeeman term in the space of states spanned by a (1,1) singlet Ψ_S^{LR} and a (1,1) triplet Ψ_T^{LR} . An applied uniform magnetic field can be used to separate the polarized triplet states energetically, so that the two-electron system remains in the branch spanned only by Ψ_S^{LR} and $\Psi_{T_0}^{LR}$. The Zeeman Hamiltonian has zero diagonal matrix elements in this branch:

$$\langle \chi_S | H_Z | \chi_S \rangle = \langle \chi_0 | H_Z | \chi_0 \rangle = 0. \quad (17)$$

and the off-diagonal matrix element is

$$\langle \Psi_S^{LR} | H_Z | \Psi_{T_0}^{LR} \rangle = -\mu_B \Delta B_z. \quad (18)$$

The x - and y -components of $\Delta \mathbf{B}$ mix the singlet with the polarized triplets

$$\begin{aligned} \langle \Psi_S^{LR} | H_Z | \Psi_{T_+}^{LR} \rangle &= \frac{\mu_B}{\sqrt{2}} (\Delta B_x + i \Delta B_y) \\ \langle \Psi_S^{LR} | H_Z | \Psi_{T_-}^{LR} \rangle &= -\frac{\mu_B}{\sqrt{2}} (\Delta B_x - i \Delta B_y). \end{aligned} \quad (19)$$

Since the polarized triplet states are split off by the uniform Zeeman field, transitions to these states are suppressed.

The triplets are mixed among themselves by the total magnetic field

$$\langle \Psi_{T_0}^{LR} | H_Z | \Psi_{T_{\pm}}^{LR} \rangle = -\frac{\mu_B}{\sqrt{2}} (B_x \pm i B_y). \quad (20)$$

Again, this mixing is suppressed because of the finite Zeeman energy from B_{tot} .

To summarize, under the action of an applied magnetic field \tilde{S}_{++}^{LR} mixes only with \tilde{T}_{++}^{LR} and \tilde{S}_{--}^{LR} mixes only with \tilde{T}_{--}^{LR} . In the $+-$ branch, \tilde{S}_{+-}^{LR} mixes only with \tilde{T}_{+-}^{LR} , while \tilde{S}_{-+}^{LR} mixes only with \tilde{T}_{-+}^{LR} . Each unpolarized (1,1) state only mixes with one other unpolarized (1,1) state, which is important in spin blockade.

F. Spin blockade in multi-valley Si QDs

Spin blockade occurs when the electrons occupy the (1,1) state with spin/valley structure incompatible with

the structure of available (0,2) states. In such case upon changing the detuning from (1,1) regime to nominally (0,2) regime the tunneling of one of the electrons into the right dot is suppressed, and the charge state of the DQD remains as (0,2). In the single-valley case this happens when we have a (1,1) triplet, from which we cannot adiabatically evolve (by changing the detuning) into a high-energy (0,2) triplet (which involves a higher orbital state). In the multi-valley case the situation is more complicated.

We first consider the $++$ branch, which is described by the Hamiltonian H_{++} . For $\delta \ll \delta_c$ the eigenstates of this Hamiltonian are \tilde{S}_{++}^{RR} , \tilde{S}_{++}^{LR} and \tilde{T}_{++}^{LR} . As the detuning is swept adiabatically from $\delta \ll \delta_c$ to $\delta \gg \delta_c$, the singlet \tilde{S}_{++}^{LR} evolves into \tilde{S}_{++}^{RR} , while the triplet \tilde{T}_{++}^{LR} remains unchanged. In other words, the (1,1) singlet evolves into the (0,2) singlet, while the (1,1) triplet remains in the (1,1) configuration. Spin blockade in the $++$ branch is the same as in GaAs. An identical argument applies for the $--$ branch.

For states from the $+-$ branch, spin blockade is rather subtle and interesting. Consider the singlet branch, described by the Hamiltonian H_{+-}^S of Eq. (13). The eigenstates of the this branch in the (0,2) and the far-detuned (1,1) regimes are respectively \tilde{S}_{+-}^{RR} and

$$\begin{aligned} \tilde{S}_{sym}^{LR} &= \frac{1}{\sqrt{2}} (\tilde{S}_{+-}^{LR} + \tilde{S}_{-+}^{LR}) \\ \tilde{S}_{anti}^{LR} &= \frac{1}{\sqrt{2}} (\tilde{S}_{+-}^{LR} - \tilde{S}_{-+}^{LR}). \end{aligned} \quad (21)$$

In the regime of $\delta \sim \delta_c$, only \tilde{S}_{+-}^{RR} and \tilde{S}_{sym}^{LR} are tunnel-coupled. Therefore, as the detuning is swept from $\delta - \delta_c \ll 0$ to $\delta - \delta_c \gg 0$, the ground state evolves from \tilde{S}_{sym}^{LR} into \tilde{S}_{+-}^{RR} , while \tilde{S}_{anti}^{LR} remains unchanged in energy.

For the $+-$ triplet branch, described by the Hamiltonian H_{+-}^T of Eq. (14), the eigenstates in the far-detuned regimes of $\delta \ll \delta_c$ and $\delta \gg \delta_c$ are \tilde{T}_{+-}^{RR} and

$$\begin{aligned} \tilde{T}_{sym} &= \frac{1}{\sqrt{2}} (\tilde{T}_{+-}^{LR} + \tilde{T}_{-+}^{LR}) \\ \tilde{T}_{anti} &= \frac{1}{\sqrt{2}} (\tilde{T}_{+-}^{LR} - \tilde{T}_{-+}^{LR}). \end{aligned} \quad (22)$$

As the detuning is swept from $\delta \ll \delta_c$ to $\delta \gg \delta_c$, the anti-symmetric state \tilde{T}_{anti}^{LR} evolves into \tilde{T}_{+-}^{RR} while \tilde{T}_{sym}^{LR} remains unchanged. This is the opposite of what happens in the $+-$ singlet branch.

The operation of the qubit entails initialization of a (0, 2) state. When \tilde{S}_{++}^{RR} is initialized and the detuning is swept from $\delta \gg \delta_c$ to $\delta \ll \delta_c$, this state evolves into \tilde{S}_{sym}^{LR} . Under the action of an inhomogeneous magnetic field this state can only mix with the triplet \tilde{T}_{sym}^{LR} . On the other hand, when \tilde{T}_{+-}^{RR} is initialized and the detuning is swept from $\delta \gg \delta_c$ to $\delta \ll \delta_c$, this state evolves into \tilde{T}_{anti}^{LR} , which, in an inhomogeneous magnetic field, can only mix with the triplet \tilde{S}_{anti}^{LR} . Therefore, as in the $++$

and $--$ branches, each state that is initialized in the (0,2) configuration only mixes with one other state when the detuning is swept to move the system into the (1,1) configuration, and spin blockade is still possible.

Under the action of an inhomogeneous magnetic field \tilde{S}_{sym}^{LR} does not mix with \tilde{T}_{anti}^{LR} , and \tilde{T}_{sym}^{LR} does not mix with \tilde{S}_{anti}^{LR} . If this mixing had been possible, spin blockade in the $+-$ branch would have been lifted. In such a situation one could have initialized \tilde{S}_{+-}^{RR} , swept the detuning so that this state evolved to \tilde{S}_{sym}^{LR} , then \tilde{S}_{sym}^{LR} would have mixed with \tilde{T}_{anti}^{LR} , and \tilde{T}_{anti}^{LR} would have evolved back to \tilde{T}_{+-}^{RR} . Under such circumstances read-out of the charge state of the right dot would not have given any indication of whether mixing had occurred in the (1,1) configuration.

The above analysis shows that spin blockade for the $+-$ states has the same outcomes as for the $++$ and $--$ states, although the way it occurs is far from obvious. Each initialized unpolarized state mixes with only one other state. In effect, spin blockade for each branch occurs in the same way as in GaAs.

We note that spin blockade is related to the so-called supertriplet and supersinglet states discussed by Palyi and Burkard in the context of graphene quantum dots.⁷⁵ In the context of Si quantum dots studied in this work, there are 16 states in the (1,1) configuration. Inspection of Fig. 6 shows that, when the detuning is swept from $\delta \ll \delta_c$ to $\delta \gg \delta_c$, 10 of these states do not change to the (0,2) configuration: the nine triplets \tilde{T}_{++}^{LR} , \tilde{T}_{--}^{LR} , and \tilde{T}_{sym}^{LR} as well as the singlet \tilde{S}_{anti}^{LR} . These are the 10 *supertriplet* states identified in Ref. 75. The 6 *supersinglet* states, which do switch to the (0,2) configuration, are the singlets \tilde{S}_{++}^{LR} , \tilde{S}_{--}^{LR} , and \tilde{S}_{sym}^{LR} , plus the three triplets \tilde{T}_{anti}^{LR} .

G. Hyperfine-induced valley mixing

The hyperfine magnetic field can be written as

$$\mathbf{B}_{nuc} = \sum_i \mathcal{A} \nu_i \mathbf{I}_i \delta(\mathbf{r} - \mathbf{R}_i). \quad (23)$$

This is a contact interaction, it is short ranged, thus it can mix states with different valley composition. As above, only \tilde{S} and \tilde{T}^0 mix. A detailed calculation shows that states from the $++$ branch do not mix with states from the $--$ branch under the influence of the nuclear field. Within the $+-$ branch, consider initialization of a (0,2) state. The singlet evolves into \tilde{S}_{sym} and the triplet evolves into \tilde{T}_{anti} . These states do not mix under the influence of the Overhauser field. The only mixing is between \tilde{S}_{sym} and \tilde{T}_{sym} , and between \tilde{S}_{anti} and \tilde{T}_{anti} .

States from the $+-$ branch can mix with those from the $++$ and $--$ branches. Some of these states cross, therefore they can be close enough in energy to be mixed. However the time scale for this process is on the order

of 0.3-1 μ s, whereas experiment uses rapid adiabatic passage, in which the system generally remains in the (1,1) regime for a relatively short time (up to a few tens of ns), thus mixing of states between different branches will be avoided at the points where the $--$ and $+-$ levels cross (see Fig 6.) At $\delta \ll \delta_c$, for mixing between different branches to be avoided, we need $\Delta \gg |B_{nuc}|$, which is satisfied by any Δ an order of magnitude larger than a few neV.

Moreover, the ^{29}Si can be isotopically purified, reducing the hyperfine-induced valley mixing as much as is needed. Therefore we expect this valley mixing to have little or no effect on spin blockade, so that the picture of spin blockade in single-valley systems is appropriate for the operation of Si spin qubits.

H. Operations of singlet-triplet qubits in multi-valley Si QDs

We have so far discussed the spectrum of the Si DQD and its different structure as compared to the simpler one-valley analogous system in GaAs. Our analysis of the spectrum has shown that various possibilities exist for doing an experiment analogous to that of Petta *et al*² and implementing a singlet-triplet qubit in a Si DQD. Depending on the magnitude of the valley splitting, different experimental outcomes may be expected. With these insights we examine in this subsection the specifics of each step in a full experiment analogous to Ref. 2 from initialization to measurement.

In Fig. 6 we show the full spectrum of the DQD including all Zeeman split triplets. If $\tilde{\Delta}$ is large, pulsed manipulation and measurement can be done reliably for singlet-triplet spin qubits in a Si DQD in the same way as in GaAs. For $\tilde{\Delta} \gg k_B T$ one can load \tilde{S}_{--}^{RR} , sweep the detuning to change this state into \tilde{S}_{--}^{LR} , which can mix only with \tilde{T}_{--}^{RR} . In other words one loads the (0,2) singlet belonging to the $--$ branch and carry out the same experiment with the same outcomes as in GaAs. In the presence of a hyperfine field the probability of return in this case will be the same as that measured in the GaAs quantum coherent experiments. If the sample is isotopically purified, the inhomogeneous field and timing of the experiment can be controlled so that the probability of return matches that found in the GaAs case.

It is more interesting to examine the case when the valley splitting is of the order of $k_B T$ (though this case may make quantum information processing less practical), so that any one of six initial states may be loaded. The initial state may belong to any of the $++$, $+-$ or $--$ singlet branches. Once this state is loaded, as the detuning is varied the system may go through any of the three anticrossings in Fig. 6. Yet, since the magnetic field does not mix valleys, once a state has been initialized in a certain branch, it will remain in that branch. As above, one can initialize \tilde{S}_{--}^{RR} and carry out the experiment as in GaAs. In principle, the same could be

done with \tilde{S}_{++}^{RR} . As for the $+-$ states, \tilde{S}_{+-}^{RR} as well as the three \tilde{T}_{+-}^{RR} states can be loaded. The state \tilde{S}_{+-}^{RR} will evolve into \tilde{S}_{sym}^{LR} as the detuning is swept, and this state can mix only with the $\tilde{T}_{sym}^{0,LR}$ unpolarized triplet. The state $\tilde{T}_{+-}^{0,RR}$ will evolve into $\tilde{T}_{anti}^{0,LR}$, which can mix only with \tilde{S}_{anti}^{LR} . Therefore, if any of the singlet or unpolarized triplet states is initialized, the outcome of sweeping the detuning will be the same as in GaAs. As for the polarized triplet states $\tilde{T}_{+-}^{\pm,RR}$, they are split off by a uniform Zeeman field that exceeds the inhomogeneous Zeeman field by a large amount by construction. The time scale for these states to be mixed with anything else by the inhomogeneous Zeeman field is thus extremely long, and much longer than the time of the experiment. As a result these states will always have a probability of return of 1. Overall, it is as if a series of parallel qubits exist in one double dot system, and for small valley splittings one could load any of them (with the possible exception of the higher-energy polarized triplet states).

This analysis demonstrates that an experiment analogous to Ref. 2 is probably feasible, except in Si it will be carried out on a series of parallel qubits. It remains to be determined to what extent this multiplicity is an impediment to quantum computation. While single-qubit operations are formally still possible even with the multiplicity introduced by the valleys, when $\tilde{\Delta}$ is comparable to $k_B T$ one can no longer be certain of initializing fiducially into a particular state. For example, there is now a finite probability of loading the triplet state $T_{+-}^{RR,0}$. This is an important consideration in two-qubit operations, which rely on the Coulomb interaction between the charge distributions of two adjacent qubits. If one has two qubits but cannot control with full certainty whether a singlet or a triplet is loaded in each of them, two-qubit operations would not be possible. Therefore, for a singlet-triplet quantum computer to work, it is imperative that $\tilde{\Delta}$ be much greater than $k_B T$.

I. Other types of qubits

Given the additional degree of freedom present in silicon, it is natural to ask whether silicon quantum dots offer multiple possibilities for implementing and initializing qubits. We discuss in this subsection two other possibilities different from the situation considered thus far, and show that, based on our current understanding and on the current ability to manipulate Si QDs in the laboratory, these alternatives cannot produce a practical qubit.

Firstly, it is evident from our discussion that the only way one can be certain of initializing a particular state in the $(0, 2)$ configuration without prior knowledge of valley splitting is to apply a strong homogeneous magnetic field so as to push the triplet $\tilde{T}_{+-}^{+,RR}$ below all the other states by an amount greatly exceeding $k_B T$. The detuning can then be altered and one electron will tunnel to

form the state $\tilde{T}_{+-}^{+,LR}$. In order to mix this state with another state it will be necessary to reduce the magnetic field greatly so that this state is close enough in energy to another state and the inhomogeneous magnetic can mix them. In addition, the three triplet states can only be mixed by a uniform transverse magnetic field, but not by an inhomogeneous field. In the end we have a 4-level system that has complicated and sometimes hard to control couplings, making it impractical for quantum information processing applications.

One could also consider using the valley degree of freedom to construct a qubit, in other words to employ the two valley-split states as a two level system and attempt to perform operations on it. In this case the same initialization problems described above are present. In addition, there is practically no control over the valley splitting and correspondingly no control over single qubits: there is no way to rotate one qubit coherently and controllably once it is initialized. The interesting paradox in this situation is that one could, in principle, implement two-qubit operations by using the exchange interaction provided by the valley-exchange Coulomb integral. This valley-exchange Coulomb integral has been discussed above and could be used to rotate states with different valley character into each other. Nevertheless, given the little amount of control over the valley splitting, and given that neither theory nor experiment have been able to determine the exact size of this exchange parameter, this would be a highly impractical method at present.

V. IDENTIFYING VALLEY-SPLIT STATES

To implement a qubit in a reliable manner we need to determine whether the condition $\tilde{\Delta} \gg k_B T$ is satisfied. Since in general $\tilde{\Delta}$ is not known there is some uncertainty in the initialization process. At present there is no simple *smoking-gun* experiment to determine whether a pair of states indeed constitute a valley-split pair, thus it is likely that in order to establish this fact unambiguously several checks need to be performed on them. We show below that two variations of the quantum coherent experiment described above² can also help estimate the magnitude of the valley splitting. If a singlet-triplet qubit is implemented in Si, the two methods outlined below (the quantum coherent experiment and the simplified experiment) can be carried out and checked against each other and against other methods of measuring the valley splitting for consistency.

A. Estimating the valley splitting in a double quantum dot

We have identified three loading/mixing channels in this work, namely the $--$, $+-$ and $++$ branches of the two-electron two-dot spectrum. Here we will demon-

strate that a magnetic field can be used to estimate the value of the valley splitting, taking advantage of the differences in dynamics between different channels. The magnetic field applied in the experiment consists of a large homogeneous part (this is not a necessary condition since the main purpose of a large uniform field is to separate out the polarized triplet states and simplify the system dynamics in the mixing regime) and a small inhomogeneous part mixing singlet and triplet states. For the purposes of this experiment, high magnetic field means the uniform part of the field must be much larger than its inhomogeneous part. For example, in experiments on GaAs the inhomogeneous field is due to the nuclei, and it is always much smaller than the uniform field, since the nuclear field in GaAs is of the order of a few mT while the applied uniform field is of the order of 100 mT. In Si the inhomogeneous field may also have to be applied, since the hyperfine field can be made vanishingly small.

We have discussed the fact that different initialized states have different probabilities of return at high magnetic fields. The average probability of return thus depends on the loading probabilities of the individual states. For the remainder of this subsection it is helpful to refer to Fig. 4. Sweeping a uniform magnetic field changes the loading probability of the polarized triplet states $\tilde{T}_{+-}^{+,RR}$ and $\tilde{T}_{+-}^{-,RR}$. This change in the loading probability alters the return probability, which can be measured experimentally. Therefore the valley splitting $\tilde{\Delta}$ can be estimated by sweeping a uniform applied magnetic field and studying the average probability of return.

For zero and very low fields, the Zeeman energy $E_Z < 2\tilde{\Delta}$, so that the two electrons should be initialized into the ground singlet state \tilde{S}_{--}^{RR} with the highest probability. As the magnetic field is increased $\tilde{T}_{+-}^{+,RR}$ eventually drops below \tilde{S}_{--}^{RR} . These two levels cross when $E_Z = 2\tilde{\Delta}$. In Fig. 11 we plot the loading and return probabilities against the magnetic field for $\tilde{\Delta} \gg k_B T$ in (a) and $\tilde{\Delta} \approx k_B T$ in (b). In both cases the probability of loading \tilde{S}_{--}^{RR} and \tilde{T}^0 will be very close to 1/2 at the crossing point when $E_Z = 2\tilde{\Delta}$. At this point the Zeeman splitting, which is known, is equal to twice the valley splitting. As the crossing point is approached, the average probability of return increases quickly, and at the crossing point the average probability of return is approximately halfway between its low-field and high-field values. For $\tilde{\Delta} = 0.1$ meV, the crossing occurs at $B = 1.76$ T and the halfway point is at $B = 1.63$ T. For $\tilde{\Delta} = 0.01$ meV, the crossing happens at $B = 0.176$ T and the halfway point is at $B = 0.17$ T. The identification of the magnetic field for this mid point thus gives a reliable estimate of the value of valley splitting $2\tilde{\Delta} = E_Z$ as long as $2\tilde{\Delta} > k_B T$.

If $2\tilde{\Delta} \ll k_B T$, the return probability will not change much as one sweeps the uniform magnetic field. The increased loading of $\tilde{T}_{+-}^{+,RR}$ compensated by the reduced loading into $\tilde{T}_{+-}^{-,RR}$ state. We cannot know $\tilde{\Delta}$ in this case, but we can know $\tilde{\Delta} \ll k_B T$, which is sufficient to

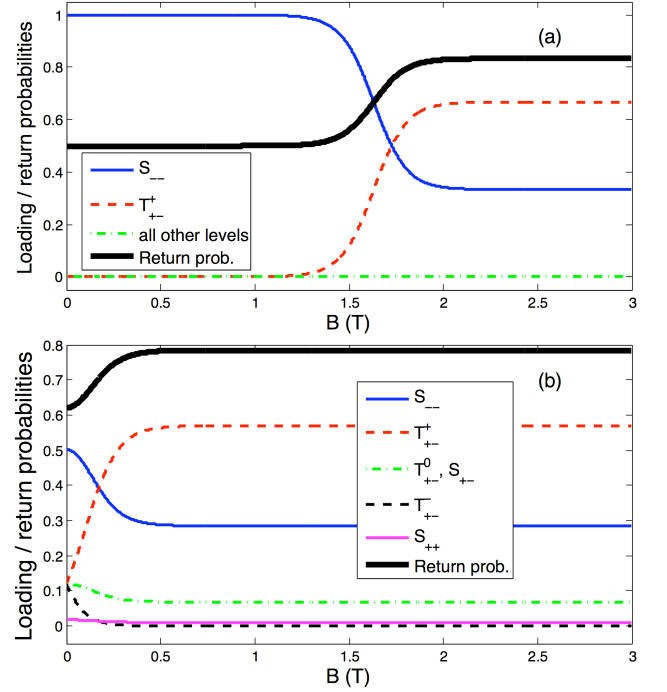


Figure 11: Loading probabilities of different levels and total return probability as a function of B for $T=100\text{mK}$ and (a) $\tilde{\Delta}=0.1\text{meV}$ and (b) $\tilde{\Delta}=0.01\text{meV}$.

determine the feasibility of qubit implementation. Thus the overall change/no-change of return probability also gives a clear indication whether $\tilde{\Delta}$ is larger than $k_B T$ or not.

B. A simplified experiment

An alternative approach to measure $\tilde{\Delta}$ is to use a two-electron single quantum dot and probe its ground state while sweeping the magnetic field. The basic idea here again relies on the detection of the magnetic field at which the ground state undergoes a singlet-triplet transition. We are indebted to discussions with Malcolm Carroll for this idea.

This single-dot experiment requires charge sensing. One should adjust the gate potential in such a way that the dot contains two electrons, so that we can refer once more to the spectrum of the doubly-occupied single dot as in Fig. 4. One can then perform tunnelling spectroscopy to determine the spectrum of the QD, and identify the ground state. At zero applied field the ground state should be a \tilde{S}_{--} singlet. As the applied field is increased, the ground state remains to be the singlet and barely changes in energy with the field, until it switches to $\tilde{T}_{+-}^{+,RR}$, beyond which the ground state energy would decrease linearly with the increasing field. This singlet-triplet transition in the ground state occurs when $E_Z = 2\tilde{\Delta}$. Therefore, recording the B-field dependence of

the ground state energy and identifying the B-field for the singlet-triplet transition should give us a reliable estimate of the valley splitting in this quantum dot. This description also shows that the experiment can be reformulated alternatively as a transport (resonant tunnelling) experiment. Recent experimental work on Si QDs⁷ suggests that this experiment is feasible at present.

C. Interface roughness

In this work we have assumed $\tilde{\Delta}$ to be a real number. In general $\tilde{\Delta}$ is complex^{70,76} and is characterized by an amplitude and a phase. Interface roughness will introduce into the problem an additional random potential. Such a random potential would yield a correction to $\tilde{\Delta}$ and could make the amplitude and phase of $\tilde{\Delta}$ different in the two dots. This would enable intervalley tunneling during interdot transitions, which could in principle affect two-dot dynamics, in particular the operations of a singlet-triplet qubit.

In current devices interface roughness is characterized by 1-2 atomic steps every few tens of nm. The potential step at the interface in a MOSFET is approximately 3 eV.⁷⁸ The random potential due to interface roughness will be considerably less than 3 eV, and is typically taken to be a small perturbation.⁷⁸ We expect the matrix element for intervalley tunneling to be considerably smaller than the matrix element for intravalley tunneling. Since the experimental scheme for implementing singlet-triplet qubits relies on rapid adiabatic passage, intervalley tunneling is a small renormalization of the energy spectrum, which remains qualitatively the same as that discussed above. The one exception is that the spacing of levels near an avoided crossing will be somewhat smaller. Therefore we do not expect singlet-triplet qubits implemented in experiment analogous to Ref. 2 to be strongly affected by interface roughness. The rich physics of this complex situation will be discussed in detail in a future publication.⁷⁹

VI. SUMMARY AND CONCLUSIONS

We have demonstrated in this work that the valley degree of freedom is of crucial importance in spin qubit architectures involving Si quantum dots. The multiplicity of the ground state fundamentally alters the energy level spectrum that is accessed in the implementation of single-spin and singlet-triplet qubits. Moreover, unlike in single-valley systems, the energy scale is no longer set by the confinement energy, but by the valley splitting, which is expected to be approximately one order of magnitude lower.

In single-spin qubits the only feasible option for quantum computation is to ensure $\tilde{\Delta} \gg k_B T$ and implement spin qubits in the same way as in a single-valley system such as GaAs. If the valley splitting $\tilde{\Delta}$ is on the

order of $k_B T$ or smaller, different single-electron valley eigenstates cannot be energetically distinguished, so that reliable orbital initialization cannot be realized even if spin states can be properly prepared. The consequence of non-identical orbital states, however, will make the exchange coupling between neighboring quantum dots unpredictable and dramatically increase the difficulty of two-qubit gates. Therefore spin quantum computation becomes practically impossible in this limit.

In singlet-triplet qubits, when $\tilde{\Delta} \gg k_B T$ the system is effectively a one-valley system and the problem is analogous to GaAs. When the condition $\tilde{\Delta} \gg k_B T$ is not satisfied, instead of the unambiguous initialization that is an important feature of GaAs experiments,² any one of six two-electron states may be loaded on a single dot. The avoided crossing of energy levels that is a hallmark of singlet-triplet qubits in GaAs translates into a set of three distinct anticrossings, which represent three different branches of the spectrum, each with a different valley composition. Depending on the relative values of $\tilde{\Delta}$, the Zeeman energy E_Z , and tunnel coupling \tilde{t} , these branches may interpenetrate, resulting in a rather complex experimental energy level spectrum. An applied magnetic field does not mix valley eigenstates with different valley composition. Singlets and triplets with different valley composition may mix under the action of a nuclear magnetic field, yet this mixing occurs on time scales much longer than those relevant to quantum coherent experiments. As a result, spin blockade in Si occurs in the same way as in GaAs. For $\tilde{\Delta} \gg k_B T$ the system is effectively a one-valley system and the problem is analogous to GaAs. Yet for $\tilde{\Delta}$ comparable to $k_B T$ the system could be viewed as a set of three parallel qubits that have no contact with each other. This may cause difficulties in implementing two-qubit operations.

We have shown also that other types of qubits involving the valley degree of freedom are not feasible based on our current knowledge and ability to control Si QDs in the laboratory.

Valley-split states and the magnitude of the valley splitting may be identified by sweeping a magnetic field. This can be done using charge sensing or transport of two electrons on a single quantum dot, or by performing a quantum coherent experiment on a singlet-triplet qubit in a double quantum dot. These measurements can be checked against one another.

It is ironic that the valley degeneracy of Si poses different qualitative problems for Si quantum dot spin qubits considered in this article compared with the corresponding Si:P bulk spin qubits, where valley degeneracy leads to the exchange oscillation phenomenon, making the fabrication and control of two-qubit exchange gates problematic.^{64,83} It appears that the valley degeneracy is a serious enemy of solid state spin quantum computation independent of whether one considers surface or bulk spin qubits. In fact, other solid state systems where valley degeneracy exists, such as graphene or carbon nanotubes, may also have difficulties with respect to spin qubit ar-

chitecture because of the competition between spin and valley degrees of freedom.

We stress that for a few qubits the existence of valleys closely spaced in energy is not necessarily a problem, since experiment can use trial and error and explicitly characterize each sample, ensuring that the valley splitting is sufficiently large. Nevertheless such a scheme is not scalable unless one determines a reliable way to control the valley splitting systematically. The ideal solution would be to develop a quantitatively precise control over valley splitting so that it can routinely be engineered to be large. Unfortunately, our theoretical understanding of valley splitting near Si surface is rather poor, and even experimentally characterizing it through direct measurement of the energy splitting is very hard.⁵¹ Designing samples with large valley splitting thus remains an elusive task.

Future work must consider scaling up singlet-triplet qubits⁹ as well as the full implications of the valley degree of freedom on such a scheme. The effect of charge noise and its possible interplay with the valley degree of freedom is also an important issue that may affect the operation of Si spin qubits, and must be duly considered.

Acknowledgments

We would like to thank M. S. Carroll for suggesting to us the simplified single-dot experiment for measuring the valley splitting. We acknowledge enlightening discussions with Jason Kestner, Neil Zimmerman, J.M. Taylor, Ted Thorbeck, M.P. Lilly, Erik Nielsen, Lisa Tracy, Malcolm Carroll, H. W. Jiang, Matt House, Mark Eriksson, Mark Friesen, S.N. Coppersmith, C. B. Simmons, A.T. Hunter, R. Joynt, Q. Niu and Zhenyu Zhang. This work is supported by LPS-NSA-CMTC. LC also acknowledges support from the Homing programme of the Foundation for Polish Science supported by the EEA Financial Mechanism.

Appendix A: Matrix elements

The interdot tunneling matrix element t has a single-particle part t_0 and a Coulomb-interaction (enhancement) part s , and we write it as $t = t_0 + s$. Starting with the wave functions $|D_\xi\rangle$, the matrix elements of the Hamiltonian within the Hund-Mulliken approximation involve the following integrals

$$\begin{aligned}
t_0 &= \langle L_\xi | H_0 | R_\xi \rangle \\
k &= \langle L_\xi^{(1)} R_\xi^{(2)} | V_{ee} | L_\xi^{(1)} R_\xi^{(2)} \rangle \\
&= \langle L_\xi^{(1)} R_{-\xi}^{(2)} | V_{ee} | L_\xi^{(1)} R_{-\xi}^{(2)} \rangle \\
j &= \langle L_\xi^{(1)} R_\xi^{(2)} | V_{ee} | L_\xi^{(2)} R_\xi^{(1)} \rangle \\
&= \langle L_\xi^{(1)} R_{-\xi}^{(2)} | V_{ee} | L_\xi^{(2)} R_{-\xi}^{(1)} \rangle \\
s &= \langle L_\xi^{(1)} L_\xi^{(2)} | V_{ee} | L_\xi^{(1)} R_\xi^{(2)} \rangle \\
&= \langle L_\xi^{(1)} L_{-\xi}^{(2)} | V_{ee} | L_\xi^{(1)} R_{-\xi}^{(2)} \rangle \\
u &= \langle D_\xi^{(1)} D_\xi^{(2)} | V_{ee} | D_\xi^{(1)} D_\xi^{(2)} \rangle \\
&= \langle D_\xi^{(1)} D_{-\xi}^{(2)} | V_{ee} | D_\xi^{(1)} D_{-\xi}^{(2)} \rangle.
\end{aligned} \tag{A1}$$

We shall refer to these as the bare matrix elements. On an asymmetric double dot we have to allow for the energies on the left and right dots, ε_L and ε_R , to be different, as explained in the text. When one switches from $\{|L\rangle, |R\rangle\}$ to the orthogonal basis spanned by $\{|\tilde{L}\rangle, |\tilde{R}\rangle\}$, the matrix elements of the Hamiltonian involve the following integrals, which are expressed in terms of the bare matrix elements introduced above:

$$\begin{aligned}
\tilde{\varepsilon}_L &= \frac{\varepsilon_L + g^2 \varepsilon_R - 2gt_0}{1 - 2lg + g^2} \\
\tilde{\varepsilon}_R &= \frac{\varepsilon_R + g^2 \varepsilon_L - 2gt_0}{1 - 2lg + g^2} \\
\tilde{t}_0 &= \frac{t_0(1 + g^2) - g(\varepsilon_L + \varepsilon_R)}{1 - 2lg + g^2} \\
\tilde{k} &= \frac{k(1 + g^4) - 4gs(1 + g^2) + 4g^2j + 2g^2u}{(1 - 2lg + g^2)^2} \\
\tilde{j} &= \frac{j(1 + g^4) - 4gs(1 + g^2) + 2g^2(k + j + u)}{(1 - 2lg + g^2)^2} \\
\tilde{s} &= \frac{s(1 + 6g^2 + g^4) - g(1 + g^2)(2j + k + u)}{(1 - 2lg + g^2)^2} \\
\tilde{u} &= \frac{u(1 + g^4) - 4gs(1 + g^2) + 4g^2j + 2g^2(k + 2j)}{(1 - 2lg + g^2)^2}.
\end{aligned} \tag{A2}$$

Appendix B: Coulomb integrals

This subsection is devoted to the evaluation of Coulomb integrals in 3D using Fourier transformation. In SI units $\epsilon \equiv 4\pi\epsilon_0\epsilon_r$, where ϵ_0 is the permittivity of free space and ϵ_r the relative permittivity. The first step is to define Fourier transform pairs as

$$\begin{aligned} f(\mathbf{r}) &= \int \frac{d^3k}{(2\pi)^3} e^{-i\mathbf{k}\cdot\mathbf{r}} F(\mathbf{k}) \\ F(\mathbf{k}) &= \int d^3r e^{i\mathbf{k}\cdot\mathbf{r}} f(\mathbf{r}). \end{aligned} \quad (\text{B1})$$

We will require the transform of $f(\mathbf{r}) = 1/r$, for which $F(\mathbf{k}) = 4\pi/k^2$. Most generally, we wish to evaluate the integral

$$I(\mathbf{P}, \mathbf{Q}) = \frac{1}{\pi^3 a^4 b^2} \int d^3r_1 \int d^3r_2 \frac{e^{-\frac{(x_1-P_x)^2+(y_1-P_y)^2}{a^2} - \frac{(z_1-P_z)^2}{b^2}} e^{-\frac{(x_2-Q_x)^2+(y_2-Q_y)^2}{a^2} - \frac{(z_2-Q_z)^2}{b^2}}}{|\mathbf{r}_1 - \mathbf{r}_2|} \quad (\text{B2})$$

We write the term $1/|\mathbf{r}_1 - \mathbf{r}_2|$ as a Fourier expansion

$$\frac{1}{|\mathbf{r}_1 - \mathbf{r}_2|} = \frac{4\pi}{(2\pi)^3} \int d^3k_2 \frac{e^{-i\mathbf{k}_2\cdot(\mathbf{r}_1-\mathbf{r}_2)}}{k_2^2} = \frac{1}{2\pi^2} \int d^3k_2 \frac{e^{-i\mathbf{k}_2\cdot(\mathbf{r}_1-\mathbf{r}_2)}}{k_2^2}. \quad (\text{B3})$$

Next we Fourier transform all the other terms (Gaussians) entering $I(\mathbf{P}, \mathbf{Q})$. First we take the z -dependent terms

$$\begin{aligned} e^{-\frac{(z_1-P_z)^2}{b^2}} &= \frac{b}{2\sqrt{\pi}} \int dk_{1z} e^{-ik_{1z}z_1} e^{-\frac{b^2k_{1z}^2}{4}} e^{ik_{1z}P_z} \\ e^{-\frac{(z_2-Q_z)^2}{b^2}} &= \frac{b}{2\sqrt{\pi}} \int dk_{3z} e^{-ik_{3z}z_2} e^{-\frac{b^2k_{3z}^2}{4}} e^{ik_{3z}Q_z}. \end{aligned} \quad (\text{B4})$$

which gives us for $I(\mathbf{P}, \mathbf{Q})$

$$I = \iiint d^3r_1 d^3r_2 d^3k_2 dk_{1z} dk_{3z} \frac{d^3r_1 d^3r_2 d^3k_2 dk_{1z} dk_{3z}}{8\pi^6 a^4} e^{-\frac{(\mathbf{r}_{1\perp}-\mathbf{P}_{\perp})^2}{a^2}} e^{-\frac{(\mathbf{r}_{2\perp}-\mathbf{Q}_{\perp})^2}{a^2}} \frac{e^{-i\mathbf{k}_2\cdot(\mathbf{r}_1-\mathbf{r}_2)}}{k_2^2} e^{-ik_{1z}(z_1-P_z)} e^{-ik_{3z}(z_2-Q_z)} e^{-\frac{b^2(k_{1z}^2+k_{3z}^2)}{4}} \quad (\text{B5})$$

Next we Fourier transform the x and y -dependent terms

$$\begin{aligned} e^{-\frac{(\mathbf{r}_{1\perp}-\mathbf{P}_{\perp})^2}{a^2}} &= \frac{a^2}{4\pi} \iint d^2k_{1\perp} e^{-i\mathbf{k}_{1\perp}\cdot(\mathbf{r}_{1\perp}-\mathbf{P}_{\perp})} e^{-\frac{a^2k_{1\perp}^2}{4}} \\ e^{-\frac{(\mathbf{r}_{2\perp}-\mathbf{Q}_{\perp})^2}{a^2}} &= \frac{a^2}{4\pi} \iint d^2k_{3\perp} e^{-i\mathbf{k}_{3\perp}\cdot(\mathbf{r}_{2\perp}-\mathbf{Q}_{\perp})} e^{-\frac{a^2k_{3\perp}^2}{4}}. \end{aligned} \quad (\text{B6})$$

The integral $I(\mathbf{P}, \mathbf{Q})$ becomes

$$\begin{aligned} I &= \iiint d^3r_1 d^3r_2 d^3k_1 d^3k_2 d^3k_3 \frac{e^{-i(\mathbf{k}_1+\mathbf{k}_2)\cdot\mathbf{r}_1} e^{-i(\mathbf{k}_3-\mathbf{k}_2)\cdot\mathbf{r}_2}}{128\pi^8} \frac{e^{i\mathbf{k}_1\cdot\mathbf{P}} e^{i\mathbf{k}_3\cdot\mathbf{Q}}}{k_2^2} e^{-\frac{(a^2k_{1\perp}^2+b^2k_{1z}^2)}{4}} e^{-\frac{(a^2k_{3\perp}^2+b^2k_{3z}^2)}{4}} \\ &= \iint \frac{d^3k_1 d^3k_2 d^3k_3}{2\pi^2} \frac{\delta(\mathbf{k}_1+\mathbf{k}_2)\delta(\mathbf{k}_3-\mathbf{k}_2)}{k_2^2} e^{i\mathbf{k}_1\cdot\mathbf{P}} e^{i\mathbf{k}_3\cdot\mathbf{Q}} e^{-\frac{(a^2k_{1\perp}^2+b^2k_{1z}^2)}{4}} e^{-\frac{(a^2k_{3\perp}^2+b^2k_{3z}^2)}{4}} \\ &= \frac{1}{2\pi^2} \int \frac{d^3k_1}{k_1^2} e^{i\mathbf{k}_1\cdot(\mathbf{P}-\mathbf{Q})} e^{-\frac{(a^2k_{1\perp}^2+b^2k_{1z}^2)}{2}}. \end{aligned} \quad (\text{B7})$$

Thus, a general three-dimensional Coulomb integral $I(\mathbf{P}, \mathbf{Q})$ can be reduced to

$$I(\mathbf{P}, \mathbf{Q}) = \frac{1}{2\pi^2} \int \frac{d^3k}{k^2} e^{i\mathbf{k}\cdot(\mathbf{P}-\mathbf{Q})} e^{-\frac{(a^2k_{\perp}^2+b^2k_z^2)}{2}} \equiv \frac{1}{2\pi^2} \int \frac{d^3k}{k^2} e^{-i\mathbf{k}\cdot\mathbf{R}} e^{-\frac{(a^2k_{\perp}^2+b^2k_z^2)}{2}}. \quad (\text{B8})$$

The integral depends only on the difference $\mathbf{R} = \mathbf{Q} - \mathbf{P}$. If \mathbf{R} is in the xy -plane we obtain

$$I(\mathbf{R}) = \int_0^\infty dk_{\perp} e^{-\frac{(a^2-b^2)k_{\perp}^2}{2}} J_0(k_{\perp}R) \text{Erfc}\left(\frac{bk_{\perp}}{\sqrt{2}}\right). \quad (\text{B9})$$

In 2D, i.e. as $b \rightarrow 0$, we have $I_{2D}(0) = \frac{1}{a} \sqrt{\frac{\pi}{2}}$.

In Hund-Mulliken problems we typically require evaluation of four bare Coulomb integrals (direct and exchange, on-site repulsion, plus an additional term), namely

$$\begin{aligned}
k &= \frac{e^2}{\epsilon} I(-X_0 \hat{\mathbf{x}}, X_0 \hat{\mathbf{x}}) \equiv \frac{e^2}{\epsilon} I(2X_0 \hat{\mathbf{x}}) \\
j &= \frac{e^2}{\epsilon} l^2 I(X_0 \hat{\mathbf{x}}, X_0 \hat{\mathbf{x}}) \equiv \frac{e^2}{\epsilon} l^2 I(0) \\
u &= \frac{e^2}{\epsilon} I(X_0 \hat{\mathbf{x}}, X_0 \hat{\mathbf{x}}) \equiv \frac{e^2}{\epsilon} I(0) \\
s &= \frac{e^2}{\epsilon} l I(-X_0 \hat{\mathbf{x}}, 0) \equiv \frac{e^2}{\epsilon} l I(X_0 \hat{\mathbf{x}}).
\end{aligned} \tag{B10}$$

Appendix C: Matrix elements in a magnetic field

In a magnetic field the wave function of each of the double dot acquires an additional phase, and we write them as $L_{\pm m}$, $R_{\pm m}$

$$\begin{aligned}
L_{\pm m} &= e^{-iyX_0/2l_B^2} L_{\pm} \\
R_{\pm m} &= e^{iyX_0/2l_B^2} R_{\pm}.
\end{aligned} \tag{C1}$$

The magnetic length is $l_B = \sqrt{\hbar/eB}$. We also introduce the Larmor frequency $\omega_L = eB/2m$, the effective frequency $\omega = \sqrt{\omega_0^2 + \omega_L^2}$ and the parameter $b_m = \sqrt{1 + \omega_L^2/\omega_0^2}$. The in-plane dot radius a , dimensionless interdot separation d and wave function overlap l all change to a_m , d_m , l_m , which are given by

$$\begin{aligned}
a_m &= a/\sqrt{b_m} \\
d_m &= d\sqrt{b_m} \\
l_m &= e^{-d^2(2b_m-1/b_m)}.
\end{aligned} \tag{C2}$$

The Coulomb integral I , introduced in the previous section, also changes to I_m , in which all the parameters are replaced by their corresponding expressions in a magnetic field, so $a \rightarrow a_m$ and so forth. The Coulomb matrix elements change as follows

$$\begin{aligned}
k_m &= \frac{e^2}{\epsilon} I_m(2X_0 \hat{\mathbf{x}}) \\
j_m &= \frac{e^2}{\epsilon} l_m^2 I_m\left(-\frac{iX_0 a_m^2}{l_B^2} \hat{\mathbf{y}}\right) \\
u_m &= \frac{e^2}{\epsilon} I_m(0) \\
s_m &= \frac{e^2}{\epsilon} l_m I_m\left(X_0 \hat{\mathbf{x}} - \frac{iX_0 a_m^2}{2l_B^2} \hat{\mathbf{y}}\right).
\end{aligned} \tag{C3}$$

The bare tunneling parameter t_0 changes to $e^{-\frac{X_0^2 a_m^2}{4l_B^2}} t_m$. Following the same pattern above, t_m is found from t_0 by replacing a with a_m and so forth.

Appendix D: Valley-exchange Coulomb integral

The valley-exchange Coulomb integral for the right dot located at \mathbf{R}_R , which we shall call j_v , is

$$j_v = \int d^3 r_1 \int d^3 r_2 R_z^{*(1)} R_z^{*(2)} V_{ee} R_z^{(1)} R_z^{(2)}. \tag{D1}$$

Let the wave functions for the two valleys z and \bar{z} (for particle i) be

$$\begin{aligned} R_z^{(i)} &= \frac{1}{\pi^{3/4}(a^2b)^{1/2}} e^{-\frac{(x_i-X_0)^2}{2a^2}} e^{-\frac{y_i^2}{2a^2}} e^{-\frac{z_i^2}{2b^2}} e^{i\mathbf{k}_z \cdot (\mathbf{r}_i - \mathbf{R}_R)} u_z(\mathbf{r}_i) \\ R_{\bar{z}}^{(i)} &= \frac{1}{\pi^{3/4}(a^2b)^{1/2}} e^{-\frac{(x_i-X_0)^2}{2a^2}} e^{-\frac{y_i^2}{2a^2}} e^{-\frac{z_i^2}{2b^2}} e^{-i\mathbf{k}_z \cdot (\mathbf{r}_i - \mathbf{R}_R)} u_{\bar{z}}(\mathbf{r}_i), \end{aligned} \quad (\text{D2})$$

where $\mathbf{k}_z = k_0 \hat{\mathbf{z}}$. For this calculation it makes no difference if we set $\mathbf{R}_R = 0$, meaning $X_0 = 0$, which will be done henceforth. The lattice-periodic part of the wave function (i.e. unit-cell wave function) can be written as

$$u_\xi(\mathbf{r}) = \sum_{\mathbf{K}} c_{\mathbf{K}}^\xi e^{i\mathbf{K} \cdot \mathbf{r}},$$

where $\xi = z, \bar{z}$ is the valley index. The aim is to reduce this integral to the form of $\text{expression} \times I(\mathbf{P}, \mathbf{Q})$ as calculated above. First,

$$R_z^{*(1)} R_{\bar{z}}^{*(2)} V_{ee} R_{\bar{z}}^{(1)} R_z^{(2)} = \frac{1}{\pi^3 a^4 b^2} \frac{e^2}{\epsilon |\mathbf{r}_1 - \mathbf{r}_2|} e^{-\frac{x_1^2+y_1^2}{a^2} - \frac{z_1^2}{b^2}} e^{-2i\mathbf{k}_z \cdot (\mathbf{r}_1 - \mathbf{r}_2)} e^{-\frac{x_2^2+y_2^2}{a^2} - \frac{z_2^2}{b^2}} u_z^*(\mathbf{r}_1) u_{\bar{z}}(\mathbf{r}_1) u_{\bar{z}}^*(\mathbf{r}_2) u_z(\mathbf{r}_2). \quad (\text{D3})$$

We expand the lattice-periodic wave functions as

$$\begin{aligned} u_z^*(\mathbf{r}_1) &= \sum_{\mathbf{K}_1} c_{\mathbf{K}_1}^{z*} e^{-i\mathbf{K}_1 \cdot \mathbf{r}_1} \\ u_{\bar{z}}(\mathbf{r}_1) &= \sum_{\mathbf{K}_3} c_{\mathbf{K}_3}^{\bar{z}} e^{i\mathbf{K}_3 \cdot \mathbf{r}_1} \\ u_{\bar{z}}^*(\mathbf{r}_2) &= \sum_{\mathbf{K}_2} c_{\mathbf{K}_2}^{\bar{z}*} e^{-i\mathbf{K}_2 \cdot \mathbf{r}_2} \\ u_z(\mathbf{r}_2) &= \sum_{\mathbf{K}_4} c_{\mathbf{K}_4}^z e^{i\mathbf{K}_4 \cdot \mathbf{r}_2} \\ u_z^*(\mathbf{r}_1) u_{\bar{z}}(\mathbf{r}_1) u_{\bar{z}}^*(\mathbf{r}_2) u_z(\mathbf{r}_2) &= \sum_{\mathbf{K}_1, \mathbf{K}_2, \mathbf{K}_3, \mathbf{K}_4} c_{\mathbf{K}_1}^{z*} c_{\mathbf{K}_3}^{\bar{z}} c_{\mathbf{K}_2}^{\bar{z}*} c_{\mathbf{K}_4}^z e^{-i(\mathbf{K}_1 - \mathbf{K}_3) \cdot \mathbf{r}_1} e^{-i(\mathbf{K}_2 - \mathbf{K}_4) \cdot \mathbf{r}_2} \\ &= \sum_{\mathbf{K}_1, \mathbf{K}_2, \boldsymbol{\kappa}_1, \boldsymbol{\kappa}_2} c_{\mathbf{K}_1}^{z*} c_{\mathbf{K}_1 - \boldsymbol{\kappa}_1}^{\bar{z}} c_{\mathbf{K}_2}^{\bar{z}*} c_{\mathbf{K}_2 - \boldsymbol{\kappa}_2}^z e^{-i\boldsymbol{\kappa}_1 \cdot \mathbf{r}_1} e^{-i\boldsymbol{\kappa}_2 \cdot \mathbf{r}_2}, \end{aligned}$$

where we have introduced $\boldsymbol{\kappa}_1 = \mathbf{K}_1 - \mathbf{K}_3$ and $\boldsymbol{\kappa}_2 = \mathbf{K}_2 - \mathbf{K}_4$. Now we can re-express the integrand in the valley-exchange integral (abbreviating $\sum \equiv \sum_{\mathbf{K}_1, \mathbf{K}_2, \boldsymbol{\kappa}_1, \boldsymbol{\kappa}_2}$)

$$R_z^{*(1)} R_{\bar{z}}^{*(2)} V_{ee} R_{\bar{z}}^{(1)} R_z^{(2)} = \frac{\sum c_{\mathbf{K}_1}^{z*} c_{\mathbf{K}_2}^{\bar{z}*} c_{\mathbf{K}_1 - \boldsymbol{\kappa}_1}^{\bar{z}} c_{\mathbf{K}_2 - \boldsymbol{\kappa}_2}^z}{\pi^3 a^4 b^2} e^{-\frac{x_1^2+y_1^2}{a^2} - \frac{z_1^2}{b^2}} e^{-i(\boldsymbol{\kappa}_1 + 2\mathbf{k}_z) \cdot \mathbf{r}_1} \frac{e^2}{\epsilon |\mathbf{r}_1 - \mathbf{r}_2|} e^{-\frac{x_2^2+y_2^2}{a^2} - \frac{z_2^2}{b^2}} e^{-i(\boldsymbol{\kappa}_2 - 2\mathbf{k}_z) \cdot \mathbf{r}_2}. \quad (\text{D4})$$

Abbreviate $\boldsymbol{\kappa}_1 + 2\mathbf{k}_z = \bar{\boldsymbol{\kappa}}_1$ and $\bar{\boldsymbol{\kappa}}_2 = \boldsymbol{\kappa}_2 - 2\mathbf{k}_z$

$$R_z^{*(1)} R_{\bar{z}}^{*(2)} V_{ee} R_{\bar{z}}^{(1)} R_z^{(2)} = \frac{\sum c_{\mathbf{K}_1}^{z*} c_{\mathbf{K}_2}^{\bar{z}*} c_{\mathbf{K}_1 - \boldsymbol{\kappa}_1}^{\bar{z}} c_{\mathbf{K}_2 - \boldsymbol{\kappa}_2}^z}{\pi^3 a^4 b^2} \left(e^{-\frac{x_1^2+y_1^2}{a^2} - \frac{z_1^2}{b^2}} e^{-i\bar{\boldsymbol{\kappa}}_1 \cdot \mathbf{r}_1} \frac{e^2}{\epsilon |\mathbf{r}_1 - \mathbf{r}_2|} e^{-\frac{x_2^2+y_2^2}{a^2} - \frac{z_2^2}{b^2}} e^{-i\bar{\boldsymbol{\kappa}}_2 \cdot \mathbf{r}_2} \right). \quad (\text{D5})$$

The integrand is almost in the form we want it, except we need to complete the square in the Gaussians. To shorten the algebra a little we note that the only sizable terms in the sum over reciprocal lattice wave vectors will have $\bar{\kappa}_{1x} = \bar{\kappa}_{1y} = \bar{\kappa}_{2x} = \bar{\kappa}_{2y} = 0$. All the rest of the terms are exponentially suppressed, or vanish because of the cubic symmetry in the Bloch state coefficients $c_{\mathbf{K}}$. So we only need to complete the square in the z -terms.

$$\begin{aligned} \frac{1}{b^2} (z_1^2 + ib^2 \bar{\kappa}_{1z}) &= \frac{1}{b^2} \left[\left(z_1 + \frac{ib^2 \bar{\kappa}_{1z}}{2} \right)^2 + \frac{b^4 \bar{\kappa}_{1z}^2}{4} \right] \\ \frac{1}{b^2} (z_2^2 + ib^2 \bar{\kappa}_{2z}) &= \frac{1}{b^2} \left[\left(z_2 + \frac{ib^2 \bar{\kappa}_{2z}}{2} \right)^2 + \frac{b^4 \bar{\kappa}_{2z}^2}{4} \right]. \end{aligned} \quad (\text{D6})$$

Therefore the valley exchange Coulomb integral can be expressed as

$$j_v = \frac{e^2}{\epsilon} \sum_{\mathbf{K}_1, \mathbf{K}_2, \boldsymbol{\kappa}_1, \boldsymbol{\kappa}_2} c_{\mathbf{K}_1}^{z*} c_{\mathbf{K}_2}^{\bar{z}*} c_{\mathbf{K}_1 - \boldsymbol{\kappa}_1}^{\bar{z}} c_{\mathbf{K}_2 - \boldsymbol{\kappa}_2}^z e^{-\frac{b^2(\bar{\kappa}_{1z}^2 + \bar{\kappa}_{2z}^2)}{4}} I \left[\frac{-ib^2(\bar{\kappa}_{1z} - \bar{\kappa}_{2z})}{2} \hat{\mathbf{z}} \right]. \quad (\text{D7})$$

Using the result for the integral I found above and $\Delta\bar{\kappa}_z = \bar{\kappa}_{1z} - \bar{\kappa}_{2z}$

$$I\left[-\frac{ib^2\Delta\bar{\kappa}_z}{2}\hat{z}\right] = \frac{1}{\pi} \int_0^\infty dk_\perp k_\perp e^{-\frac{a^2k_\perp^2}{2}} \int_{-\infty}^\infty dk_z \frac{e^{\frac{k_z b^2 \Delta\bar{\kappa}_z}{2}} e^{-\frac{b^2k_z^2}{2}}}{k_\perp^2 + k_z^2} \quad (D8)$$

$$k_z^2 - k_z \Delta\bar{\kappa}_z = \left(k_z - \frac{\Delta\bar{\kappa}_z}{2}\right)^2 - \frac{\Delta\bar{\kappa}_z^2}{4}.$$

So we redefine $k_z \rightarrow k_z + \frac{\Delta\bar{\kappa}_z}{2}$ in the above integral without affecting the limits of integration

$$I\left[-\frac{ib^2\Delta\bar{\kappa}_z}{2}\hat{z}\right] = \frac{e^{\frac{b^2\Delta\bar{\kappa}_z^2}{8}}}{\pi} \int_0^\infty dk_\perp k_\perp e^{-\frac{a^2k_\perp^2}{2}} \int_{-\infty}^\infty dk_z \frac{e^{-\frac{b^2k_z^2}{2}}}{k_\perp^2 + (k_z + \frac{\Delta\bar{\kappa}_z}{2})^2} \quad (D9)$$

where

$$ak_\perp = q_\perp$$

$$bk_z = q_z$$

$$b\Delta\bar{\kappa}_z = \Delta q_z \quad (D10)$$

so that

$$I\left[-\frac{ib^2\Delta\bar{\kappa}_z}{2}\hat{z}\right] = \frac{e^{\frac{\Delta q_z^2}{8}} b}{\pi a^2} \int_0^\infty dq_\perp q_\perp e^{-\frac{q_\perp^2}{2}} \int_{-\infty}^\infty dq_z \frac{e^{-\frac{q_z^2}{2}}}{q_\perp^2 \left(\frac{b^2}{a^2}\right) + (q_z + \frac{\Delta q_z}{2})^2}. \quad (D11)$$

We examine the overall exponential prefactor. The exponent is

$$\begin{aligned} \frac{b^2\Delta\bar{\kappa}_z^2}{8} - \frac{b^2(\bar{\kappa}_{1z}^2 + \bar{\kappa}_{2z}^2)}{4} &= \frac{b^2(\bar{\kappa}_{1z}^2 + \bar{\kappa}_{2z}^2 - 2\bar{\kappa}_{1z}\bar{\kappa}_{2z}) - 2b^2(\bar{\kappa}_{1z}^2 + \bar{\kappa}_{2z}^2)}{8} \\ &= -\frac{b^2(\bar{\kappa}_{1z} + \bar{\kappa}_{2z})^2}{8} = -\frac{b^2(\kappa_{1z} + \kappa_{2z})^2}{8}. \end{aligned} \quad (D12)$$

This prefactor therefore has no dependence on k_0 . For the final step in the evaluation of the integral we examine which reciprocal lattice vectors make a sizable contribution. The coefficients $c_{\mathbf{K}}^\xi$ for Si were calculated in Ref. 84 using a pseudopotential method. Equation (D12) above tells us we want $\kappa_{1z} + \kappa_{2z} = 0$. The first possibility is $\kappa_{1z} = \kappa_{2z} = 0$, with $\Delta q_z = 4bk_0$, yielding

$$\sum \approx \sum_{\mathbf{K}_1, \mathbf{K}_2} c_{\mathbf{K}_1}^{z*} c_{\mathbf{K}_1}^{\bar{z}} c_{\mathbf{K}_2}^{\bar{z}*} c_{\mathbf{K}_2}^z \approx 0.01. \quad (D13)$$

The second possibility is $\kappa_{1z} = -\kappa_{2z}$, in which case $\Delta q_z = 2b\kappa_{1z} + 4bk_0$. These terms cancel exactly because of lattice symmetry.

The valley-exchange Coulomb integral is approximately

$$j_v \approx \frac{e^2}{\epsilon a} \left(\sum \right) \left\{ \frac{b}{\pi a} \int_0^\infty dq_\perp q_\perp e^{-\frac{q_\perp^2}{2}} \int_{-\infty}^\infty dq_z \frac{e^{-\frac{q_z^2}{2}}}{q_\perp^2 \left(\frac{b^2}{a^2}\right) + (q_z + \frac{\Delta q_z}{2})^2} \right\} \quad (D14)$$

For $a = 8.2$ nm, $b = 3$ nm and $\epsilon \approx 7.9$, we get $\Delta q_z \approx 117$ and $(e^2/\epsilon a) \approx 22.2$ meV. The integral in brackets is evaluated using Mathematica and yields $\approx 8.5 \times 10^{-5}$, so the final result is $j_v \approx 0.02 \mu\text{eV}$.

¹ M. A. Nielsen and I. L. Chuang, *Quantum Computation and Quantum Information* (Cambridge University Press,

Cambridge, England, 2000).

- ² J. R. Petta, A. C. Johnson, J. M. Taylor, E. A. Laird, A. Yacoby, M. D. Lukin, C. M. Marcus, M. P. Hanson, and A. C. Gossard, *Science* **309**, 2180 (2005).
- ³ F. H. L. Koppens, K. C. Nowack, and L. M. K. Vandersypen, *Phys. Rev. Lett.* **100**, 236802 (2008).
- ⁴ G. Feher and E. A. Gere, *Phys. Rev.* **114**, 1245 (1959).
- ⁵ B. E. Kane, *Nature (London)* **393**, 133 (1998).
- ⁶ M. Mottonen, K. Y. Tan, K. W. Chan, F. A. Zwanenburg, W. H. Lim, C. C. Escott, J.-M. Pirkkalainen, A. Morello, C. Yang, J. A. van Donkelaar, et al., arXiv:0910.0731 (2009).
- ⁷ W. H. Lim, F. A. Zwanenburg, H. Huebl, M. Mottonen, K. W. Chan, A. Morello, and A. S. Dzurak, arXiv:0910.0576 (2009).
- ⁸ D. Loss and D. P. DiVincenzo, *Phys. Rev. A* **57**, 120 (1998).
- ⁹ J. M. Taylor, H.-A. Engel, W. Dür, P. Zoller, A. Yacoby, C. M. Marcus, and M. D. Lukin, *Nat. Phys.* **1**, 177 (2005).
- ¹⁰ E. Gallardo, L. Martinez, A. Nowak, H. van der Meulen, J. Calleja, C. Tejedor, I. Prieto, D. Granados, A. Taboada, J. Garcia, et al., 0908.1161 (2009).
- ¹¹ S. Foletti, H. Bluhm, D. Mahalu, V. Umansky, and A. Yacoby, *Nature Phys.* p. DOI: 10.1038/NPHYS1424 (2009).
- ¹² D. P. DiVincenzo, D. Bacon, J. Kempe, G. Burkard, and K. B. Whaley, *Nature* **408**, 339 (2000).
- ¹³ K. Ono, D. G. Austing, Y. Tokura, and S. Tarucha, *Science* **297**, 1313 (2002).
- ¹⁴ J. M. Elzerman, R. Hanson, L. H. Willems van Beveren, B. Witkamp, L. M. K. Vandersypen, and L. P. Kouwenhoven, *Nature* **430**, 431 (2004).
- ¹⁵ A. C. Johnson, J. R. Petta, J. M. Taylor, A. Yacoby, M. D. Lukin, M. P. Hanson, A. C. Gossard, and C. M. Marcus, *Nature* **435**, 925 (2005).
- ¹⁶ F. H. L. Koppens, J. A. Folk, J. M. Elzerman, R. Hanson, L. H. Willems van Beveren, I. T. Vink, H. P. Tranitz, W. Wegscheider, L. P. Kouwenhoven, and L. M. K. Vandersypen, *Science* **309**, 1346 (2005).
- ¹⁷ R. Hanson, L. P. Kouwenhoven, J. R. Petta, S. Tarucha, and L. M. K. Vandersypen, *Rev. Mod. Phys.* **79**, 1217 (2007).
- ¹⁸ Y. Hu, H. O. H. Churchill, D. J. Reilly, J. Xiang, C. M. Lieber, and C. M. Marcus, *Nat. Nano.* **2**, 622 (2007).
- ¹⁹ N. Shaji, C. B. Simmons, M. Thalakulam, L. J. Klein, H. Qin, H. Luo, D. E. Savage, M. G. Lagally, A. J. Rimberg, R. Joynt, et al., *Nat. Phys.* **4**, 540 (2008).
- ²⁰ D. J. Reilly, J. M. Taylor, E. A. Laird, J. R. Petta, C. M. Marcus, M. P. Hanson, and A. C. Gossard, *Phys. Rev. Lett.* **101**, 236803 (2008).
- ²¹ C. Barthel, D. J. Reilly, C. M. Marcus, M. P. Hanson, and A. C. Gossard, *Phys. Rev. Lett.* **103**, 160503 (2009).
- ²² M. Field, C. G. Smith, M. Pepper, D. A. Ritchie, J. E. F. Frost, G. A. C. Jones, and D. G. Hasko, *PRL* **70**, 1311 (1993).
- ²³ J. M. Taylor, J. R. Petta, A. C. Johnson, A. Yacoby, C. M. Marcus, and M. D. Lukin, *Phys. Rev. B* **76**, 035315 (2007).
- ²⁴ I. A. Merkulov, A. I. Efros, and M. Rosen, *Phys. Rev. B* **65**, 205309 (2002).
- ²⁵ A. Khaetskii, D. Loss, and L. Glazman, *Phys. Rev. B* **67**, 195329 (2003).
- ²⁶ W. A. Coish and D. Loss, *Phys. Rev. B* **72**, 125337 (2005).
- ²⁷ W. Yao, R.-B. Liu, and L. J. Sham, *Phys. Rev. B* **74**, 195301 (2006).
- ²⁸ W. M. Witzel and S. Das Sarma, *Phys. Rev. B* **74**, 035322 (2006).
- ²⁹ S. K. Saikin, W. Yao, and L. J. Sham, *Phys. Rev. B* **75**, 125314 (2007).
- ³⁰ W. A. Coish, J. Fischer, and D. Loss, *Phys. Rev. B* **77**, 125329 (2008).
- ³¹ L. Cywiński, W. M. Witzel, and S. Das Sarma, *Phys. Rev. Lett.* **102**, 057601 (2009).
- ³² L. Cywiński, W. M. Witzel, and S. Das Sarma, *Phys. Rev. B* **79**, 245314 (2009).
- ³³ D. Klauser, W. A. Coish, and D. Loss, *Phys. Rev. B* **73**, 205302 (2006).
- ³⁴ J. Danon and Y. V. Nazarov, *Phys. Rev. Lett.* **100**, 056603 (2008).
- ³⁵ G. Ramon and X. Hu, *Phys. Rev. B* **75**, 161301 (2007).
- ³⁶ M. Stopa, J. J. Krich, and A. Yacoby, *Phys. Rev. B* **81**, 041304(R) (2010).
- ³⁷ W. Yao, R.-B. Liu, and L. J. Sham, *Phys. Rev. Lett.* **98**, 077602 (2007).
- ³⁸ W. M. Witzel and S. Das Sarma, *Phys. Rev. Lett.* **98**, 077601 (2007).
- ³⁹ G. S. Uhrig, *Phys. Rev. Lett.* **98**, 100504 (2007).
- ⁴⁰ B. Lee, W. M. Witzel, and S. Das Sarma, *Phys. Rev. Lett.* **100**, 160505 (2008).
- ⁴¹ C. Tahan and R. Joynt, *Phys. Rev. B* **71**, 075315 (2005).
- ⁴² L. Asalli, H. Petrilli, R. B. Capaz, B. Koiller, X. Hu, and S. D. Sarma, preprint (2010).
- ⁴³ W. M. Witzel, X. Hu, and S. Das Sarma, *Phys. Rev. B* **76**, 035212 (2007).
- ⁴⁴ M. Prada, R. H. Blick, and R. Joynt, *Phys. Rev. B* **77**, 115438 (2008).
- ⁴⁵ A. M. Tyryshkin, J. J. L. Morton, S. C. Benjamin, A. Ardavan, G. A. D. Briggs, J. W. Ager, and S. A. Lyon, *J. Phys. Condens. Matter* **18**, S783 (2006).
- ⁴⁶ E. Abe, K. M. Itoh, J. Isoya, and S. Yamasaki, *Phys. Rev. B* **70**, 033204 (2004).
- ⁴⁷ R. Vrijen, E. Yablonovitch, K. Wang, H. W. Jiang, A. Balandin, V. Roychowdhury, T. Mor, and D. DiVincenzo, *Phys. Rev. A* **62**, 012306 (2000).
- ⁴⁸ T. B. Boykin, G. Klimeck, M. Friesen, S. N. Coppersmith, P. von Allmen, F. Oyafuso, and S. Lee, *Phys. Rev. B* **70**, 165325 (2004).
- ⁴⁹ R. R. Hayes, A. A. Kiselev, M. G. Borselli, S. S. Bui, E. T. C. III, P. W. Deelman, B. M. Maune, I. Milosavljevic, J.-S. Moon, R. S. Ross, et al., arXiv:0908.0173 (2009).
- ⁵⁰ H. W. Liu, T. Fujisawa, Y. Ono, H. Inokawa, A. Fujiwara, K. Takashina, and Y. Hirayama, *Phys. Rev. B* **77**, 073310 (2008).
- ⁵¹ E. P. Nordberg, G. A. T. Eyck, H. L. Stalford, R. P. Muller, R. W. Young, K. Eng, L. A. Tracy, K. D. Childs, J. R. Wendt, R. K. Grubbs, et al., *Phys. Rev. B* **80**, 115331 (2009).
- ⁵² T. Ferrus, M. Tanner, G. Podd, P. Chapman, and D. A. Williams, arXiv:0907.2635 (2009).
- ⁵³ S. E. S. Andresen, R. Brenner, C. J. Wellard, C. Yang, T. Hopf, C. C. Escott, R. G. Clark, A. S. Dzurak, D. N. Jamieson, et al., *Nano Lett.* **7**, 2000 (2007).
- ⁵⁴ M. Mitić, K. D. Petersson, M. C. Cassidy, R. P. Starrett, E. Gauja, A. J. Ferguson, C. Yang, D. N. Jamieson, R. G. Clark, and A. S. Dzurak, *Nanotechnology* **19**, 265201 (2008).
- ⁵⁵ I. Kuljanishvili, C. Kayis, J. F. Harrison, C. Piermarocchi, T. A. Kaplanand, S. H. Tessler, L. N. Pfeiffer, and K. W. West, *Nat. Phys.* **4**, 227 (2008).
- ⁵⁶ G. P. Lansbergen, R. Rahman, C. J. Wellard, I. Woo, J. Caro, N. Collaert, S. Biesemans, G. Klimeck, L. C. L.

- Hollenberg, and S. Rogge, Nat. Phys. **4**, 656 (2008).
- ⁵⁷ A. Fuhrer, M. Fuchsle, T. C. G. Reusch, B. Weber, and M. Y. Simmons, Nano Lett. **9**, 707 (2009).
 - ⁵⁸ A. R. Stegner, C. Boehme, H. Huebl, M. Stutzmann, K. Lips, and M. S. Brandt, Nature Phys. **2**, 835 (2006).
 - ⁵⁹ S. J. Angus, A. J. Ferguson, A. S. Dzurak, and R. G. Clark, Nano Lett. **7**, 2051 (2007).
 - ⁶⁰ L. P. Rokhinson, L. J. Guo, S. Y. Chou, and D. C. Tsui, Phys. Rev. Lett. **87**, 166802 (2001).
 - ⁶¹ S. Goswami, K. A. Slinker, M. Friesen, L. M. McGuire, J. L. Truitt, C. Tahan, L. J. Klein, J. O. Chu, P. M. Mooney, D. W. van der Weide, et al., Nat. Phys. **3**, 41 (2007).
 - ⁶² W. H. Lim, H. Huebl, L. H. W. van Beveren, S. Rubanov, P. G. Spizzirri, S. J. Angus, R. G. Clark, and A. S. Dzurak, Appl. Phys. Lett. **94**, 173502 (2009).
 - ⁶³ E. P. Nordberg, H. L. Stalford, R. Young, G. A. Ten Eyck, K. Eng, L. A. Tracy, K. D. Childs, J. R. Wendt, R. K. Grubbs, J. Stevens, et al., Appl. Phys. Lett. **95**, 202102 (2009).
 - ⁶⁴ B. Koiller, X. Hu, and S. Das Sarma, Phys. Rev. Lett. **88**, 027903 (2001).
 - ⁶⁵ C. J. Wellard and L. C. L. Hollenberg, Phys. Rev. B **72**, 085202 (2005).
 - ⁶⁶ T. Ando, Phys. Rev. B **19**, 3089 (1979).
 - ⁶⁷ M. Friesen and S. N. Coppersmith, arXiv:0902.0777 (2009).
 - ⁶⁸ K. Lai, T. M. Lu, W. Pan, D. C. Tsui, S. Lyon, J. Liu, Y. H. Xie, M. Mühlberger, and F. Schäffler, Phys. Rev. B **73**, 161301 (2006).
 - ⁶⁹ K. Takashina, Y. Ono, A. Fujiwara, Y. Takahashi, and Y. Hirayama, Phys. Rev. Lett. **96**, 236801 (2006).
 - ⁷⁰ A. Saraiva, M. Calderon, X. Hu, S. Das Sarma, and B. Koiller, Phys. Rev. B **80**, 081305 (2009).
 - ⁷¹ T. B. Boykin, G. Klimeck, M. A. Eriksson, M. Friesen, S. N. Coppersmith, P. von Allmen, F. Oyafuso, and S. Lee, Appl. Phys. Lett. **84**, 115 (2004).
 - ⁷² M. O. Nestoklon, L. E. Golub, and E. L. Ivchenko, Phys. Rev. B **73**, 235334 (2006).
 - ⁷³ S. Srinivasan, G. Klimeck, and L. P. Rokhinson, Appl. Phys. Lett. **93**, 112102 (2008).
 - ⁷⁴ H. O. H. Churchill, F. Kuemmeth, J. W. Harlow, A. J. Bestwick, E. I. Rashba, K. Flensberg, C. H. Stwertka, T. Taychatanapat, S. K. Watson, and C. M. Marcus, Phys. Rev. Lett. **102**, 166802 (2009).
 - ⁷⁵ A. Pályi and G. Burkard, Phys. Rev. B **80**, 201404 (2009).
 - ⁷⁶ Y. Hada and M. Eto, Jpn. J. Appl. Phys. **43**, 7329 (2004).
 - ⁷⁷ D. Culcer, L. Cywiński, Q. Li, X. Hu, and S. Das Sarma, Phys. Rev. B **80**, 205302 (2009).
 - ⁷⁸ T. Ando, A. B. Fowler, and F. Stern, Rev. Mod. Phys. **54**, 437 (1982).
 - ⁷⁹ D. Culcer, X. Hu, and S. Das Sarma (unpublished).
 - ⁸⁰ G. Burkard, D. Loss, and D. P. DiVincenzo, Phys. Rev. B **59**, 2070 (1999).
 - ⁸¹ J. Slater, *Quantum Theory of Molecules and Solids* (McGraw-Hill, New York, 1963).
 - ⁸² Q. Li, L. Cywiński, D. Culcer, X. Hu, and S. Das Sarma, arXiv:0906.4793 (2009).
 - ⁸³ B. Koiller, X. Hu, and S. Das Sarma, Phys. Rev. B **66**, 115201 (2002).
 - ⁸⁴ B. Koiller, R. B. Capaz, X. Hu, and S. Das Sarma, Phys. Rev. B **70**, 115207 (2004).
 - ⁸⁵ S. Lyon, private communication
 - ⁸⁶ In a recent two-electron measurement, the coherence time in GaAs QDs reaches 30 μ s after Hahn echo and $> 100 \mu$ s after multi-pulse Car-Purcell-Meiboom-Gill (CPMG) sequence (A. Yacoby, private communication.)
 - ⁸⁷ M. P. Lilly, private communication